An assessment of CMIP6 climate signals and biases in temperature, precipitation and soil moisture over Europe

Osso, A. ORCID: https://orcid.org/0000-0001-5653-4886, Craig, P. ORCID: https://orcid.org/0000-0001-9213-4599 and Allan, R. P. ORCID: https://orcid.org/0000-0003-0264-9447
(2023) An assessment of CMIP6 climate signals and biases in temperature, precipitation and soil moisture over Europe. International Journal of Climatology, 43 (12). pp. 5698-5719. ISSN 0899-8418 doi: 10.1002/joc.8169 Available at https://centaur.reading.ac.uk/112504/

Received: 2 November 2022 | Revised: 19 May 2023 | Accepted: 18 June 2023

DOI: 10.1002/joc.8169

International Journal of Climatology RMetS

RESEARCH ARTICLE

An assessment of CMIP6 climate signals and biases in temperature, precipitation and soil moisture over Europe

Albert Ossó[1] | **Philip Craig**[2] | **Richard P. Allan**[2,3]

[1]Wegener Center for Climate and Global Change, University of Graz, Graz, Austria

[2]Department of Meteorology, University of Reading, Reading, UK

[3]National Centre for Earth Observation, University of Reading, Reading, UK

Correspondence
Albert Ossó, Wegener Center for Climate and Global Change, University of Graz, Graz, Austria.
Email: albert.osso-castillon@uni-graz.at

Funding information
ERA4CS; Karl-Franzens-Universität Graz; INDECIS Project; European Union, Grant/Award Number: 690462; DLR (DE); FORMAS (SE); BMWFW (AT); IFD (DK); MINECO (ES); ANR (FR)

Abstract

The CMIP6 projections constitute the basis of our latest understanding of the climate response to anthropogenic forcing. However, there is still considerable uncertainty in the projections, especially at the regional scale. One way to constrain the uncertainty is by comparing the models historical climate change signals against observations and investigate the physical reasons for divergences. Here, we assess the signal-to-noise ratio (S/N) of surface air temperature (SAT), precipitation (PREC) and soil moisture (SM) over Europe for a set of CMIP6 historical simulations and compare them against the E-OBS observational product and the ERA5 reanalysis. We found considerable divergences between the CMIP6 ensemble mean S/N and that of E-OBS and ERA5, as well as between ERA5 and E-OBS. The latter indicates that the S/N is affected by data coverage. We show that the differences among model signals are associated with different atmospheric circulation responses. We also investigate the potential relationships between the models' signals and climatological biases, and we found evidence that the models with a warm climatological bias in southern Europe tend to have smaller SAT signals (warm less). Finally, we found no apparent relationship between SM biases and the warming signal, suggesting that the mechanism by which SM–atmosphere interactions affect climate variability does not explain the mean changes. However, there is a tendency for models with higher SM to dry faster than models with lower SM.

KEYWORDS

climate change signals, CMIP6, model biases

1 | INTRODUCTION

Reliable projections of the regional climate response to increasing greenhouse gases (GHG) are critical for adaptation planning. In the last decades, there has been enormous progress in understanding the climate response to increasing GHGs and projections based on global circulation models (GCM) have become a widespread tool to assess the future climate. The main climate modelling effort is arguably the Coupled Model Intercomparison Project (CMIP), coordinated by the World Climate Research Programme (WCRP), which is currently in

phase 6 (CMIP6) and have become the benchmark of climate research. Information distilled from the CMIP6 climate projections constitutes the basis of our latest understanding of climate change. However, the CMIP ensembles, particularly at the regional scale, are still plagued with considerable uncertainty (e.g., Deser, 2020; Foley, 2010; Giorgi & Francisco, 2000; Shepherd, 2014). The main uncertainties in identifying the real-world forced response from CMIP ensembles arise from differences in the models representation of physical processes (typically called "model uncertainty"), internal variability and scenario uncertainty (e.g., Hawkins & Sutton, 2009). For long time scales (>century and beyond), differences in the models' forced response are thought to dominate over internal variability, but at the decadal timescales (which are the most relevant for adaptation planning), both are similarly relevant (e.g., Douville et al., 2021 IPCC AR6 WG1 chapter 08, fig. 8.23).

One way to assess and potentially reduce the model and internal variability uncertainty of the climate projections is by evaluating historical simulations (simulations driven by common past observed forcing) against observations, identifying the model differences and attributing them to the particular representation of physical processes or internal variability. This approach assumes that the models better representing the observed past will better represent the future. Although this assumption might not always be valid, a comparison can still help to identify statistical relationships between the model biases of an observable variable and its trends. Several studies (e.g., Carvalho et al., 2021; Cattiaux et al., 2013; Giorgi & Coppola, 2010) show that the models' forced response depends on the model mean biases and there is some evidence that the models that better represent some aspects of the current climate (e.g., the SLP patterns) tend to simulate similar future climates (Watterson, 2019). These relationships can constitute a so-called "emergent constraint" and can be used to narrow the uncertainty due to different model responses (e.g., Brient, 2020; Hall et al., 2019).

Observational studies have shown that European mean temperatures have increased at almost twice the rate than the global average (e.g., van der Schrier et al., 2013). However, the historical trends show notable seasonal and spatial differences, with the highest warming observed in northeast Europe and Scandinavia during winter and southern Europe during summer (e.g., Ossó et al., 2022). For a global mean temperature increase of 2 K, the CMIP6 ensemble-mean projects a warming with respect to 1850–1900 in winter (summer) of 3.4 K (2.7 K) over northern Europe and Scandinavia, with a 2σ ensemble spread of 2.6 K (2.4 K). In southern Europe and the Mediterranean area, the projected warming for winter (summer) is 2 K (2.9 K) with a 2σ ensemble spread of 1 K (1 K) (IPCC AR6 Climate Atlas Gutiérrez et al., 2021). These results show that although the models agree with the sign and the general spatial structure of the trends, their magnitudes differ.

The average precipitation over Europe has not changed significantly since 1960 in the E-OBS dataset. However, at the subcontinental scale, winter precipitation has shown a small decrease in south Europe and an increase of up to 70 mm·decade^{-1} in northern Europe (Maraun, 2013). In summer, significant decreases have been observed in southern Europe and significant increases in northern Europe (van den Besselaar et al., 2013).

For a global mean temperature increase of 2 K, the CMIP6 ensemble-mean projects an increase of precipitation with respect to 1850–1900 in winter (summer) of 2.7 mm·day^{-1} (1.9 mm·day^{-1}) over northern Europe and Scandinavia with a 2σ ensemble spread of 0.7 mm·day^{-1} (0.9 mm·day^{-1}). In southern Europe and the Mediterranean area, the projected precipitation change for winter (summer) is of −1.8 mm·day^{-1} (−0.5 mm·day^{-1}) with a 2σ ensemble spread of 1.4 K (0.6 K) (IPCC AR6 Climate Atlas Gutiérrez et al., 2021). Generally, there is little agreement among models' precipitation trends, with several models showing opposite regional trends.

In this work, we examine historical (1950–2014) surface air temperature (SAT), precipitation (PREC) and soil moisture (SM) over Europe from the CMIP6 models, the ERA5 reanalysis and the E-OBS dataset to assess the emergence of climate change signals, identify robust patterns across all datasets and investigate reasons for discrepancies.

The climate change signals are identified by analysing the signal-to-noise ratio (S/N) of the timeseries, which is calculated using a regression scheme introduced by Hawkins et al. (2020) that assumes that the local force component of the variable into consideration linearly scales with the global mean surface temperature (GMST). Similar pattern scaling approaches have been widely used, including in the IPCC AR5 (Collins et al., 2013) and are justified by the evidence that the spatial pattern of change of temperature and precipitation for various forcing scenarios is often similar (e.g., Santer et al., 1990).

However, the method has some limitations that must be taken into account when interpreting the results: (1) GMST is affected by decadal and multidecadal variability, so it is not a perfect proxy of the external forcing (e.g., Lopez et al., 2014; Watterson, 2019); (2) it does not take into account possible nonlinearities of the climate system and (3) it does not take into account the impact of aerosols in modifying the local forced response (Frieler et al., 2012; Watterson & Whetton, 2013).

To the best of our knowledge, this is the first time this method has been applied to identify the S/N in CMIP6

historical simulations. Moreover, new insights into the relationships between CMIP6 signals and climatological biases over Europe are presented. In this context, we aim to answer the following questions: (1) What are the historical climate change signals of SAT, PREC and SM in CMIP6 models over Europe? Moreover, are the signals robust? (2) How do the simulated S/N compare to observations? (3) How do intermodel S/N discrepancies relate to mean biases?

2 | DATA AND METHODS

2.1 | CMIP6 models

We use data from 17 models from the Coupled Model Intercomparison Project Phase 6 (CMIP6) historical runs (Eyring et al., 2016) that are listed in Table 1. This selection of models samples a range of horizontal resolutions and modelling centres. This selection does not contain the entire CMIP6 ensemble; however, previous work shows that this number of models is adequate for sampling across a range of model physics (e.g., Allan et al., 2022; Santer et al., 2021). The r1i1p1f1 member of each model is used. "r" is the realization number and distinguishes among members of an ensemble that differ only in their initial conditions, "i" indicate the initialisation method, which in CMIP6 should invariably be assigned the value "1" except for some hindcast and forecast experiments, "p" identifies the physics version used by the model and "f" indicates the type of forcing applied. In our case, all the models are forced with the CMIP6-recommended forcing historical data from 1850 to 2014 (Eyring et al., 2016). We also use 40 members (r1i1p1 to r40i1p1) of the ACCESS-ESM1.5 models, which only differ in their initial conditions to test the impact of internal variability on the results. SM values for all CMIP6 models is provided by the variable "mrsos," which measures the water content in all phases within the upper 0.1 m of soil and is averaged over the land portion of the grid cell. However, as ERA5 provides soil moisture in the upper 0.07 m of soil, we have converted the gravimetric soil water per unit area ($kg \cdot m^{-2}$) to volumetric water content ($m^3 \cdot m^{-3}$) to enable a cleaner comparison of SM trends between models and observations (Yuan et al., 2021). This is achieved by dividing the gravimetric soil water content by the respective layer thickness (10 cm for the CMIP6 models and 7 cm for ERA5) and by the density of pure water ($1000\ kg \cdot m^{-3}$). The CMIP6 data were interpolated to a common $1.5° \times 1.5°$ grid (approximately the ensemble mean horizontal resolution) to calculate an ensemble mean and to compare to other datasets.

TABLE 1 List of historical CMIP6 simulations and their resolution

Model	Resolution	Reference
BCC-ESM1	2.8125° × 2.8125°	Wu et al. (2020)
CanESM5	2.8125° × 2.8125°	Swart et al. (2019)
AWI-ESM-1-1-LR	1.875° × 1.865°	Semmler et al. (2020)
ACCESS-CM2	1.875° × 1.25°	Bi et al. (2020)
UKESM-0-LL	1.875° × 1.25°	Sellar et al. (2020)
ACCESS-ESM1.5	1.875° × 1.25°	Ziehn et al. (2020)
CNRM-ESM2-1	1.40625° × 1.40625°	Séférian et al. (2019)
MIROC6	1.40625° × 1.40625°	Tatebe et al. (2019)
MRI-ESM2-0	1.125° × 1.125°	Yukimoto et al. (2019)
GFDL-ESM4	1.25° × 1°	Dunne et al. (2020)
FIO-ESM-2-0	1.25° × 0.9375°	Bao et al. (2020)
CMCC-ESM2	1.25° × 0.9375°	Cherchi et al. (2019)
CESM2	1.25° × 0.9375°	Danabasoglu et al. (2020)
NorESM2-MM	1.25° × 0.9375°	Seland et al. (2020)
TaiESM1	1.25° × 0.9375°	Wang et al. (2021)
MPI-ESM1-2-HR	0.9375° × 0.9375°	Mauritsen et al. (2019)
EC-EARTH3	0.703125° × 0.703125°	Döscher et al. (2021)

2.2 | Reanalysis and observations

ERA5 is the latest reanalysis product from the European Centre for Medium-Range Weather Forecasts (ECMWF), spanning from 1950 to the present (Bell et al., 2021; Hersbach et al., 2020). We use ERA5 data from 1950 to 2014, matching the end date of the CMIP6 historical runs. This reanalysis product uses the 2016 version ECMWF forecast model (Integrated Forecasting System; IFS) Cy41r2, which has three fully coupled components for the atmosphere, land and ocean waves. ERA5 uses an ensemble 4D-Var data assimilation system with 10 members that assimilate in situ observations of wind, humidity and pressure along with radiances sensitive to upper-air temperature and humidity from various satellites. The data are on a full N320 Gaussian grid with a horizontal resolution of 31 km (0.28125°) and 137 vertical levels. We use the 2-m air temperature (t2m), total precipitation (tp) and upper level (0–7 cm) SM (swvl1). We only analyse the upper SM since it is the level more strongly coupled with the atmosphere (Seneviratne et al., 2010).

We also use Europe-focused E-OBS v23.0 in this study since it is based purely on observed station data (Cornes et al., 2018). The E-OBS dataset is constructed by the European Climate Assessment and Dataset (ECA&D) project using station data provided by national meteorological agencies. The station data are interpolated to a grid using a two-stage process incorporating a deterministic model and a stochastic technique. E-OBS daily data are available on regular 0.1° and 0.25° grids. For this study, we used the daily temperature (tg) and rainfall (rr) on the 0.25° grid.

2.3 | S/N calculation

The signal-to-noise ratio (S/N) is calculated using the method described by Hawkins et al. (2020) and Ossó et al. (2022). We start by regressing seasonal climate variations onto seasonal global mean surface temperature (GMST),

$$L(t)=\alpha G(t)+b, \quad (1)$$

where $L(t)$ is the local change of a variable (e.g., temperature, precipitation) over time, $G(t)$ is GMST smoothed over 1950–2014 using a 15-year rolling mean (Ossó et al., 2022), and α and β are the linear regression coefficients. Notice that by construction, the method removes most of the influence of internal interannual variability. Thereby, $L(t)$ captures mainly the forced signal. The full 1950–2014 time period is used to incorporate a common long-running time series across both CMIP6 and observations and to calculate the anomalies. The statistical significance of the linear regression coefficients is calculated using the Wald (1943) test with a *t*-distribution of the test statistic and adjusted degrees of freedom to account for autocorrelation. GMST is calculated from each CMIP6 model near-surface air temperature (tas) when calculating S/N for each model (Hawkins & Sutton, 2012) and the CMIP6 S/N ensemble mean is calculated by averaging the S/N values of each individual model. For ERA5 we used its 2-m air temperature (t2m) to calculate GMST and S/N. The HadCRUT5 dataset (Morice et al., 2021) was used to calculate GMST when calculating S/N for E-OBS since E-OBS is a European-only dataset.

The signal (S) of a variable is simply the difference between the first and last values of the linear model $L(t)$ (i.e., $S=L(t_n)-L(t_0)$) and the noise (N) is the standard deviation of the residual between a given variable and its associated $L(t)$. This framework assumes that $\alpha G(t)$ is a good representation of the forced component of the local change. This assumption has been shown to be a reasonable approximation for temperature (Sutton et al., 2015) and extremes of temperature and precipitation (Fischer & Knutti, 2014). Since SM is strongly controlled by temperature and precipitation, it is reasonable to assume this scaling assumption also holds for SM. The resulting S/N quantifies the ratio between the forced component of the local change and its internal variability for a particular period. Here we use the qualitative classification introduced by Frame et al. (2017), which classifies S/N values as "unusual" (S/N > 1), "unfamiliar" (S/N > 2) and "unknown" (S/N > 3).

3 | EMERGENCE OF CLIMATE CHANGE SIGNALS

This section compares the S/N of SAT, PREC and SM between CMIP6, ERA5 and E-OBS.

3.1 | Surface air temperature

The JJA CMIP6 ensemble mean S/N is greater than 1 across the entire domain, with the greatest S/N values found along the west coast of Great Britain, around the Baltic Sea and on the coasts of the Black and Aegean Sea where S/N > 1.6 (Figure 1a). ERA5 S/N have a more defined structure than the CMIP6 ensemble mean with larger S/N values over southern Europe and smaller values over much of north Europe (Figure 1c). Large values (S/N > 2) are found over mountainous terrains such as the Alps, Carpathians and southeast Spain in southern Europe and the Norwegian mountain regions. This is consistent with observations from high-altitude stations in various mountainous regions (Marty & Meister, 2012; Ohmura, 2012), as discussed later. The E-OBS JJA S/N is somewhat different, with a less coherent structure (Figure 1e) and generally weaker S/N than CMIP6 and ERA5. This is likely a result of poor data coverage and quality across Europe (e.g., Prein & Gobiet, 2017), which can add nonphysical noise that aliases onto or dampen climate change signals and suggests that the emergence of climate change signals, even for SAT, is affected by data coverage. Finally, the region with S/N < 0 around Romania was previously attributed to data sparsity and homogeneity problems associated with incorporating cooler SAT from high-altitude stations (Craig & Allan, 2022).

The DJF CMIP6 ensemble mean S/N for SAT is below 1 for most of Europe but exceeds 1 along the northernmost extremities of Scandinavia, parts of south Europe and across parts of Great Britain and Ireland (Figure 1b). The smaller S/N values than in summer mainly result from a larger noise and not a smaller signal. ERA5's DJF S/N has some similarities with S/N > 1 over much of the Iberian Peninsula and Great Britain, but also large regions of

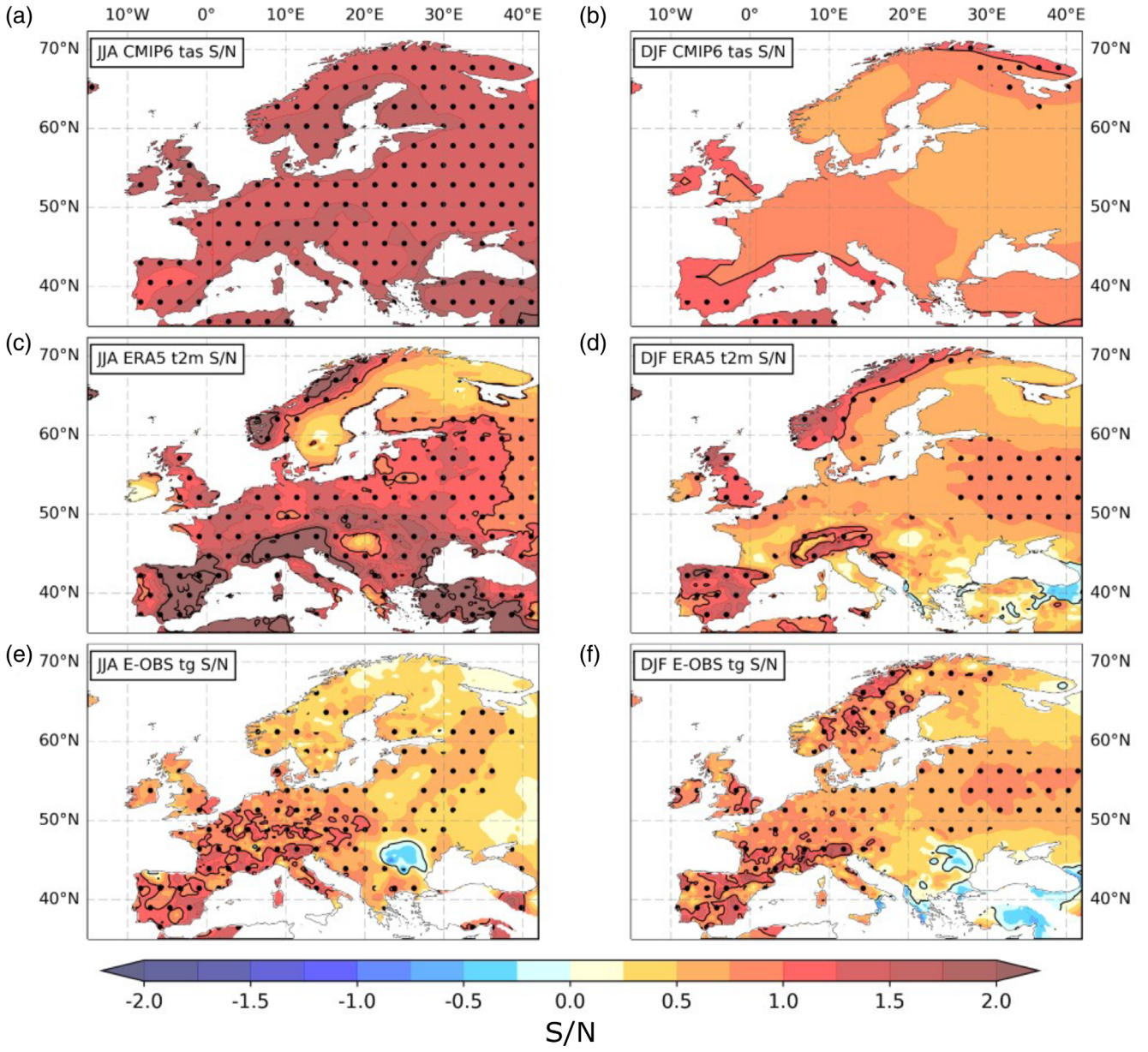

FIGURE 1 Maps of SAT S/N for (a, b) the CMIP6 ensemble mean, (c, d) ERA5 and (e, f) E-OBS for JJA and DJF calculated across 1950–2014. Yellow to red colours indicate positive S/N (increasing temperature) and blue indicate negative S/N (decreasing temperature). The stippling in (a, b) shows where two-thirds of the CMIP6 models' S/N are statistically significant at the 95% level and in (c–f) it shows where the ERA5 and E-OBS S/N are statistically significant at the 95% level. The black contours highlight the regions where $|S/N| > 1$ and $|S/N| > 2$. An additional contour is included in panel c to highlight a region where $S/N > 3$ [Colour figure can be viewed at wileyonlinelibrary.com]

$S/N > 1$ over Norway and the Alps (Figure 1d). Reasons for greater SAT change at high altitudes are detailed by Ohmura (2012). For example, the reduced quantities of snow and ice caused by warming reduce the albedo effect of the surface, enhancing warming. The DJF E-OBS S/N (Figure 1f) shows a somewhat different structure than CMIP6 and ERA5 and resembles its JJA S/N pattern. However, regions of $S/N > 1$ over the Alps, Pyrenees and small parts of Norway are consistent with ERA5.

As expected, the CMIP6 ensemble means S/N pattern is much smoother than those for each model (Figure S1, Supporting Information). In JJA, the ensemble spread (standard deviation) of S/N exceeds 0.6 across much of Europe, although it is much lower across eastern Europe (Figure S1). The large spread can be associated with differences in the model representation of the physical processes and low-frequency internal variability not removed by the regression scheme (see section 5).

The CNRM-ESM2-1 model has a S/N with a spatial structure most similar to ERA5, with a large S/N over the Iberian Peninsula, the Alps and the Norwegian coast. On the contrary, the BCC-ESM1 is most similar to E-OBS, with lower S/N over much of the continent, decreasing from the southwest (SW) to the northeast (NE). Some models have S/N > 2 across much of Europe (CESM2, CanESM5, EC-Earth3), which shows warming at a greater rate than ERA5 or E-OBS (Figure 1), but there are also two models (MPI-ESM1-2-HR and GFDL-ESM4) that have small areas with S/N < 0 in Portugal and northwest Russia, respectively.

The DJF S/N ensemble spread has a similar east/west structure to JJA: exceeding 0.6 to the west with a lower spread over eastern Europe and western Russia (Figure S2). There is much diversity in the DJF S/N patterns, with some models showing regions with S/N < 0 (ACCESS-CM2, CMCC-ESM2, FIO-ESM-2-0, GFDL-ESM4) and contrasting spatial structures such as increasing S/N from SW to NE (BCC-ESM1) and decreasing S/N of the same orientation (CNRM-ESM2-1). UKESM appears to resemble the spatial structure and values of ERA5 and E-OBS S/N the best of the CMIP6 models, with S/N > 1 over the Iberian Peninsula and the Alps, then decreasing below 1 across the rest of Europe. However, UKESM also has a high climate sensitivity and a too-cold aerosol period in the 1960s/1970s (Meehl et al., 2020; Sellar et al., 2020). However, none of the models show the same contrast in S/N between the Norwegian mountains and Sweden present in ERA5 (Figure 1d).

High-altitude regions such as the Alps and Norwegian mountains show S/N > 1 in both seasons, with an indication of the same phenomenon in ERA5 and somewhat in E-OBS (Figure 1c–f). This is in stark contrast to lower altitude regions such as the Pannonian Basin around Hungary (Ceglar et al., 2018), which has remarkably lower ERA5 S/N in both seasons compared to the surrounding mountain ranges. Ohmura (2012) explains four reasons why high-altitude regions experience warming faster than low-altitude regions. These are the cryosphere/temperature feedback, temperature amplification in an inversion layer, condensation at high altitudes releasing high levels of latent heat, and the construction of the Stefan-Boltzmann equation, which permits the temperature sensitivity of the energy balance to be amplified at the lower temperatures of high altitude.

3.2 | Precipitation

The JJA CMIP6 ensemble mean S/N for PREC does not exhibit any defined structure. The magnitudes are everywhere smaller than ±0.25 S/N (Figure 2a), indicating that there has not been any remarkable change in summer PREC over Europe. However, ERA5 and E-OBS JJA S/N (Figure 2c,e) have a different spatial structure to CMIP6, with negative S/N around the Mediterranean and positive S/N across parts of the main continent where CMIP6 has weak negative S/N—although both datasets have positive S/N across Scandinavia. ERA5 and E-OBS S/N values are small across the continent: In ERA5, there are only two small regions in Norway/Sweden and Spain with |S/N| > 1, and the E-OBS has only two tiny regions in Lapland and the Iberian Peninsula, where |S/N| > 1.

For DJF, the CMIP6 ensemble mean S/N is smaller than ±0.5 everywhere, with positive values all over Europe except over some regions of the Mediterranean coast, where small negative values are apparent (Figure 2b). Unlike JJA, the CMIP6 ensemble mean shows wetter winters for almost all of Europe. However, the S/N values are smaller than 1 everywhere. E-OBS S/N structure is similar to CMIP6 with overall positive values except over some areas of the Mediterranean coast (Figure 2f). However, the S/N structure of ERA5 is remarkably different. It is characterized by a distinct north/south split along a SW to NE diagonal where the northern region has positive and the southern region negative S/N (Figure 2d). This results in the boundary between positive and negative S/N in ERA5 being shifted further north than in E-OBS and the CMIP6 ensemble mean. These differences could partially be attributed to the persistent general model deficiency in representing the jet tilt over the North Atlantic, resulting in the jet intercepting the European continent too far south. This bias has been observed in the past (Doblas et al., 1998; Woollings, 2010) and current CMIP6 (Simpson et al., 2020) model assessments. An analysis of the individual models sea-level pressure (SLP) biases is consistent with a too zonal storm track over Europe in virtually all the models (Figures S7 and S8).

The S/N of the individual models is quite diverse, and many do not resemble the ensemble mean. In JJA, the S/N ensemble spread is high (greater than 0.6) along the coast of Norway, where the models disagree on the sign and strength of S/N (Figure S3). Some models (e.g., CanESM5, EC-Earth3, UKESM1-0-LL) have S/N > 1 in this region, but other models have S/N < 0 (e.g., ACCESS-CM2, BCC-ESM1, MIROC6). Remarkably, several models show increased PREC over southern Europe and the Mediterranean (e.g., EC-Earth3, GFDL-ESM4, ACCESS-ESM1-5, NorESM2-MM) in contradiction with observations. EC-Earth3 has the strongest positive S/N over much of Scandinavia and south Europe. CMCC-ESM2 has mostly S/N < 0, but it is generally weak compared to CanESM5's region of negative S/N around Denmark, Germany and Holland. Only MRI-ESM2-0 has a similar north/south split to ERA5 and

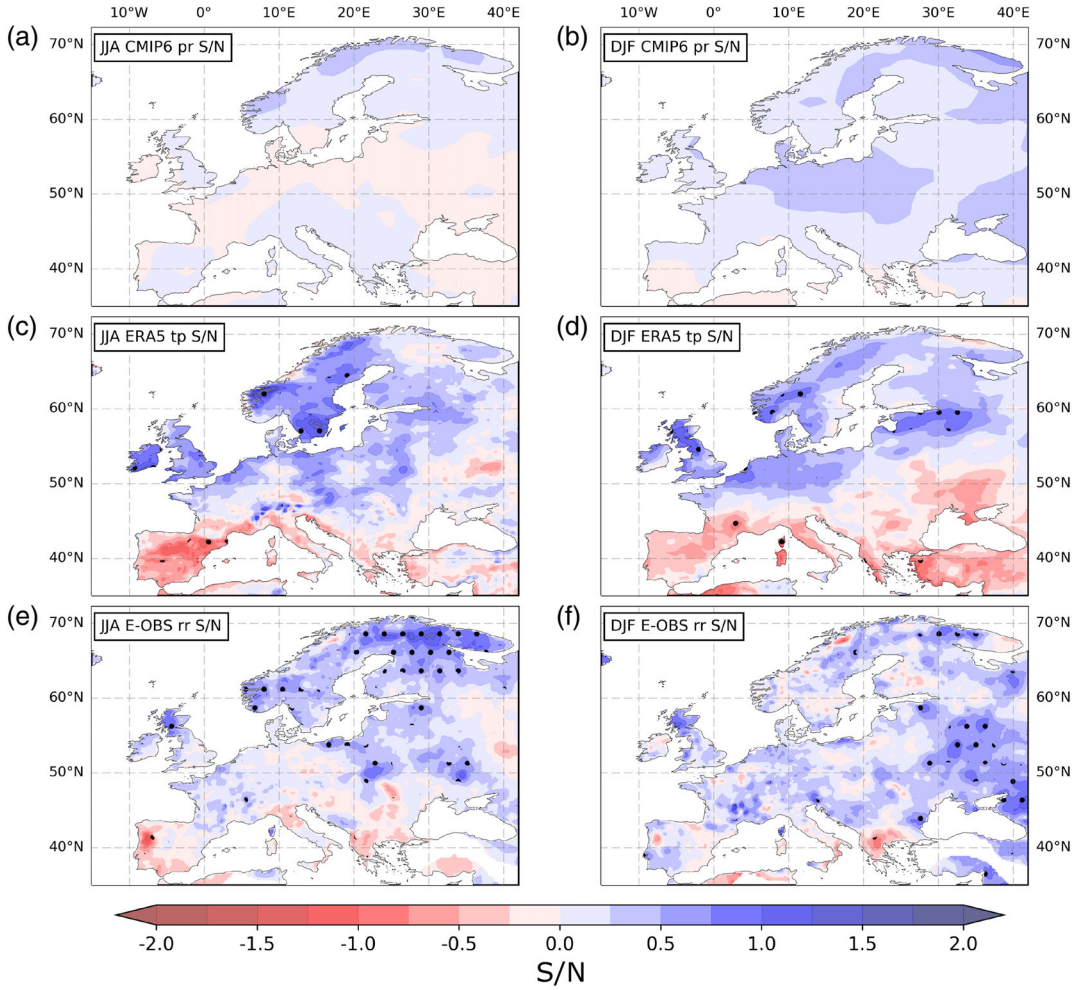

FIGURE 2 Maps of PREC S/N for (a, b) the CMIP6 ensemble mean, (c, d) ERA5 and (e, f) E-OBS for JJA and DJF calculated across 1950–2014. Blue contours indicate positive S/N (increasing precipitation) and red contours indicate negative S/N (decreasing precipitation). The stippling in (a, b) shows where two-thirds of the CMIP6 models' S/N are statistically significant at the 95% level and in (c–f) it shows where the ERA5 and E-OBS S/N are statistically significant at the 95% level. The statistical significance is calculated using the Wald (1943) test. The black contours highlight the regions where $|S/N| > 1$ and $|S/N| > 2$ [Colour figure can be viewed at wileyonlinelibrary.com]

E-OBS, with some models showing the opposite pattern of increasing PREC in the south and decreasing PREC in the north (e.g., ACCESS-ESM1-5, NorESM2-MM).

The DJF S/N ensemble spread is of a similar magnitude with that in JJA (Figure S4). The region of the largest DJF ensemble spread stretches from the Atlantic coast to the western border of Poland. This matches the large positive S/N values on the continent in AWI-ESM1-1-1-LR and CNRM-ESM2-1 compared to the negative S/N values in ACCESS-CM2, CMCC-ESM2 and MIROC6. The area of the ensemble mean S/N close to 1 around Poland (Figure 2b) is a consequence of various models with strong positive S/N but also some models with weaker S/N bringing down the ensemble mean (e.g., BCC-ESM1, NorESM2-MM). TaiESM1 has the closest S/N resemblance to ERA5's distinct north/south split, and two other models (GFDL-ESM4, NorESM2-MM) also have similar structures to ERA5. Notice that none of the models S/N resembles that of the E-OBS. Generally, the model differences in their PREC S/N patterns are coherent with the differences in their SLP signals (Figures S9 and S10), suggesting that divergent circulation changes as a response to climate change and internal variability not removed by the regression model largely determine the differences in the models PREC change.

3.3 | Soil moisture

The JJA CMIP6 ensemble mean SM S/N is negative (drying) almost everywhere in Europe apart from two tiny and isolated regions of Spain, Sicily and northwest Italy (Figure 3a). The drying increases with latitude and is

larger across northern Scandinavia, although the ensemble mean does not reach 1. SM is therefore decreasing across CMIP6 models but has yet to cross the threshold for an "unusual" climate. ERA5's SM is also mostly negative across Europe but unlike the CMIP6 ensemble mean, it has positive values over Great Britain, Ireland, Sweden and Finland, indicating an increase in SM in these areas (Figure 3c). However, only Ireland has S/N > 1, indicating that the soil has become unusually wet, consistently with the large positive JJA PREC S/N over this area in ERA5 (Figure 2c). Some mountain regions in Spain, Norway and the Alps have S/N < −1, indicating that there has been a transition to unusually dry SM in these regions. This is consistent with the amplified SAT signal over mountainous terrain in ERA5 t2m (Figure 1c). Moreover, an early snow melt and the usually thin soil of mountainous regions are likely to contribute to the strong S/N value upsetting any increase in PREC (e.g., Jasper et al., 2004). Note that northern coastal regions have a narrow band of positive S/N, which might be a consequence of the differential warming rates between the coast and the North Sea, increasing the intensity of moist advection inland during summer (Diffenbaugh et al., 2007).

The DJF S/N is negative across most of Europe except in some areas of Scandinavia and Russia, where S/N > 0 (Figure 3b). Similar to JJA, the S/N is weak across the entire domain (|S/N| < 1 everywhere). Winter SM in the CMIP6 has not transitioned into an "unusual" climate. The ERA5 SM S/N has a north/south split with S/N > 0 across the north and S/N < 0 for the south (Figure 3d), indicating an increase in SM across north Europe and drying soil across south Europe. This pattern is likely to be closely associated with the similar north/south split in ERA5 winter PREC. Mountainous regions in Spain and the Balkans have unusual levels of drying (S/N < −1). Parts of Scandinavia have S/N > 1, indicating that SM content in these regions is unusually large compared to past climate.

In JJA, the individual models exhibit a substantial diversity of SM S/N patterns, with the largest ensemble spread over Scandinavia, eastern Europe and western Russia, where several models have opposite S/N signs (Figure S5). In particular, CNRM-ESM2-1 has a very strong negative S/N (similar to its SAT S/N), and MPI-ESM2-0 and GFDL-ESM4 have weak positive S/N. As in the case of JJA S/N PREC, the models show a diversity of signals over southern Europe and the Mediterranean

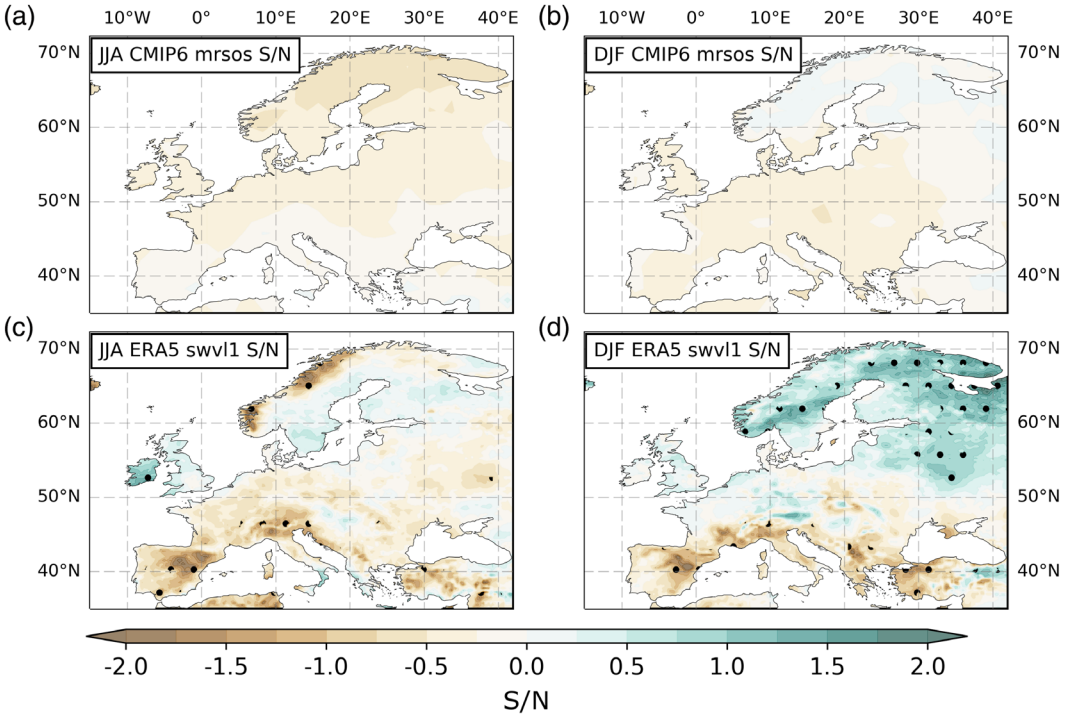

FIGURE 3 Maps of S/N for (a, b) the CMIP6 ensemble mean mrsos and (c, d) ERA5 swvl1 for JJA and DJF calculated across 1950–2014. Green contours indicate positive S/N (increasing soil moisture) and brown contours indicate negative S/N (decreasing soil moisture). The stippling in (c, d) shows where ERA5 S/N is statistically significant at the 95% level. The statistical significance is calculated using the Wald (1943) test. The same test was applied to each CMIP6 model but no grid points in the domain shown passes the same two-thirds threshold applied for Figures 1 and 2. The black contours highlight the regions where |S/N| > 1 and |S/N| > 2 [Colour figure can be viewed at wileyonlinelibrary.com]

region, with the models showing an increase in PREC (Figure S3) also showing an increase in SM (i.e., EC-Earth3, ACCESS-ESM1-5, NorESM2-MM) which is clearly at odds with observations. As for JJA PREC, MRI-ESM2-0 resembles ERA5 the most. Interestingly, in JJA, the SM patterns strongly resemble PREC in continental Europe but not Scandinavia, where several models show a substantial increase in PREC but decreasing SM. This suggests that changes in PREC strongly control continental Europe's SM changes, while over Scandinavia, other factors also have a strong impact (e.g., warming, early snow-melt).

The DJF S/N ensemble spread is greater than in JJA across the central part of the continent, with more diversity in the models S/N (Figure S6). For example, MRI-ESM1-2-0 and CanESM5 have S/N < 0 (drying SM) everywhere but FIO-ESM-2-0 and MPI-ESM1-2-HR have mostly positive S/N (increasing SM). Despite the greater ensemble spread, the Iberian Peninsula has a lower ensemble spread than in JJA, where most models have negative S/N. The north/south split in ERA5 S/N (Figure 3d) may be replicated at least partially by AWI-ESM-1-1-LR and TaiESM1 with negative S/N in south Europe and positive S/N in north Europe.

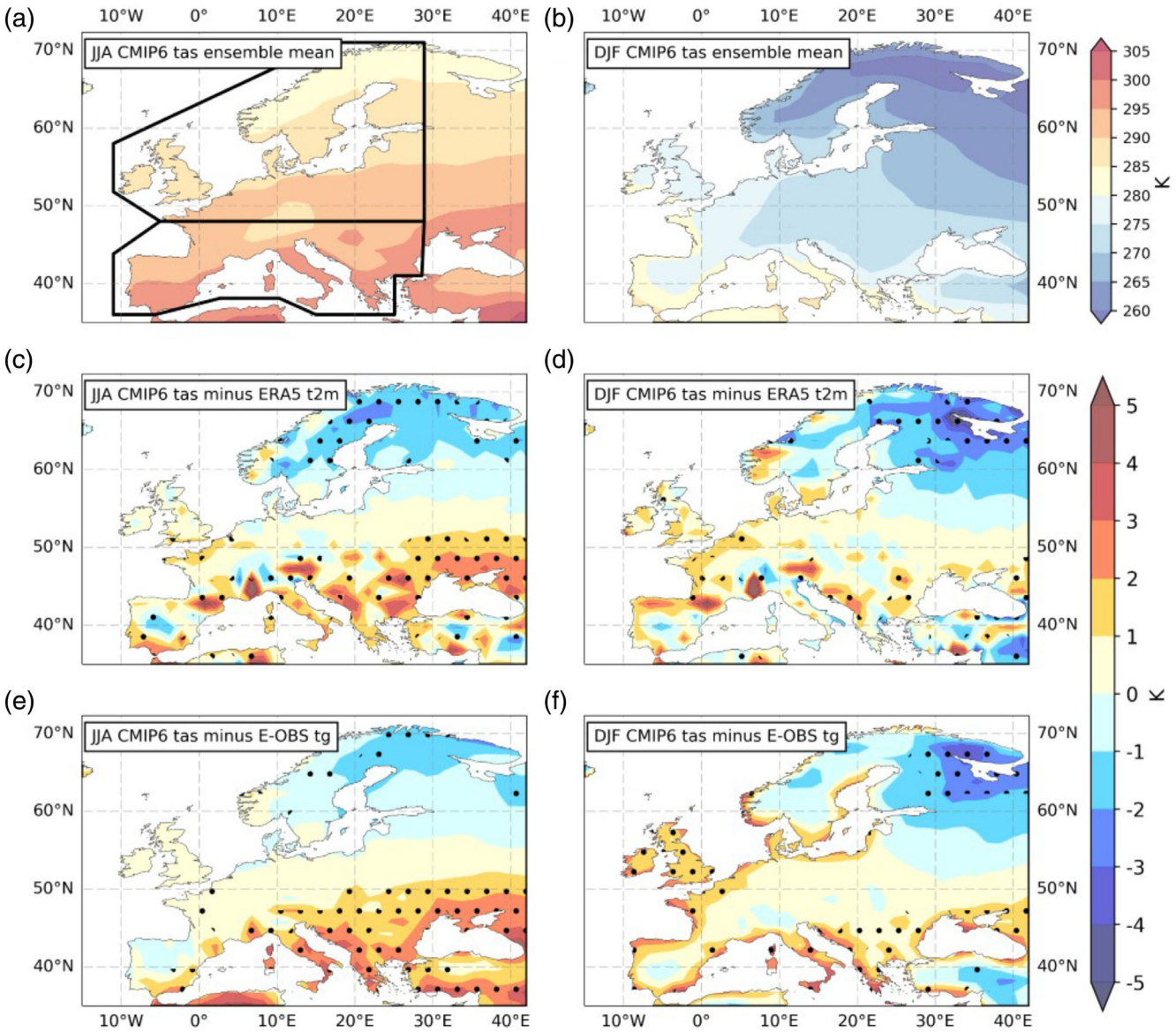

FIGURE 4 Maps of (a, b) CMIP6 ensemble climatological mean tas, (c, d) climatological bias using ERA5 t2m and (e, f) climatological bias using E-OBS for JJA and DJF calculated across 1950–2014. The biases are calculated as model minus observations, so yellow-to-red contours indicate warmer model temperatures and blue contours indicate cooler model temperatures. Stippling in (c–f) shows where at least two-thirds of the CMIP6 models agree on the sign of the climatological bias. The north and south regions used to calculate area-averages for the scatter plots are shown in (a) [Colour figure can be viewed at wileyonlinelibrary.com]

4 | LINKING SIGNAL BIASES TO MEAN BIASES

In this section, we further explore the diversity of the model signals and try to identify relationships between the model signal biases and the models mean biases. We focus in the signals (*S*) instead of in the S/N since the differences between models are primarily attributed to the differences in the signals (see Supporting Information). The purpose of this analysis is not to provide an exhaustive evaluation of model bias (which is covered in other studies) but instead to understand S/N changes in the context of mean biases to aid physical interpretation. To that aim, we calculate area-averaged climatological biases of CMIP6 SAT, PREC and SM with respect to ERA5 and E-OBS and compare those with the area-averaged signal biases (the difference between model and observed signal) across north and south Europe. These two areas are chosen based on a visual inspection of the areas subjected to similar changes across variables (Figure 4a highlights the definition of the two areas). Scatterplots between the variables of interest identify the relationships, and a correlation coefficient quantifies their strength. We only show the scatterplots showing significant relationships, but a comprehensive summary of the correlation coefficients found is given in supplemental Tables S1 and

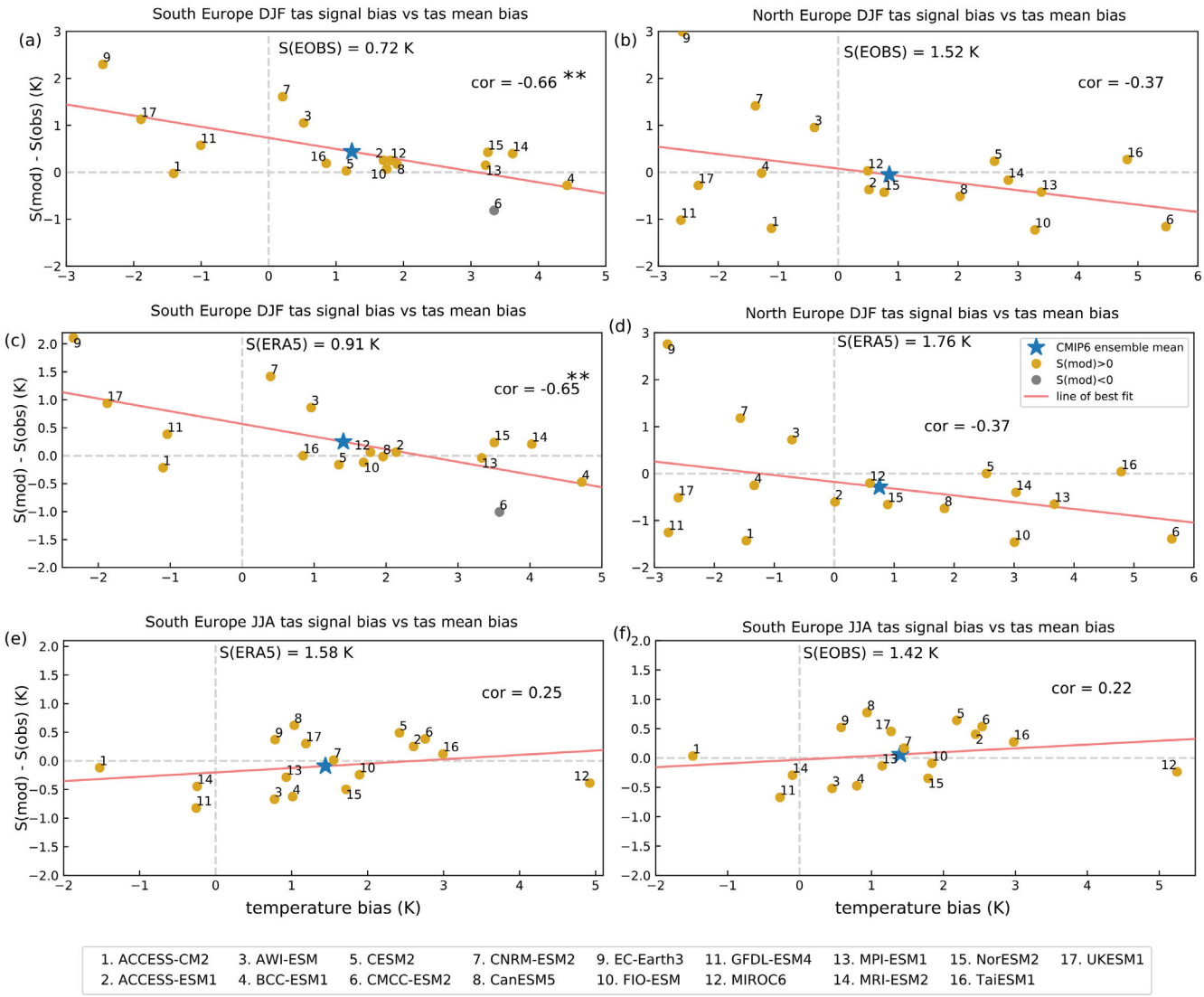

FIGURE 5 Scatter plots of area-averaged CMIP6 climatological temperature bias and signal bias for (a) south Europe DJF E-OBS, (b) north Europe DJF E-OBS, (c) south Europe DJF ERAS, (d) north Europe DJF ERAS, (e) south Europe JJA ERAS and (f) south Europe JJA E-OBS. The star indicates the climatological and signal bias for the CMIP6 ensemble mean. The red line indicates the line of best fit for the scatter points shown by gold (positive signal) or grey (negative signal) circles. The correlation coefficient between the climatological and signal biases is shown on each panel, along with the area-averaged E-OBS and ERAS signals. Asterisks (**) indicates correlation coefficients statistically significant at the 95% level [Colour figure can be viewed at wileyonlinelibrary.com]

S2. Note that a strong relationship can help to narrow the uncertainty due to differences in model responses and inform on plausible mechanisms (Brient, 2020).

4.1 | Surface air temperature

Figure 4 shows the CMIP6 ensemble SAT and the bias to ERA5 and E-OBS for JJA (left panel) and DJF (right panel). In summer, the CMIP6 ensemble mean has a warm bias in southern Europe and a cold bias in northern Europe with respect to both ERA5 (Figure 4c) and E-OBS (Figure 4e). Stippling shows where at least two-thirds of the CMIP6 models agree on the sign of the bias indicating that the bias pattern is not due to a few very warm or very cold models, but it is common among CMIP6 models. This bias pattern could be related to an SLP bias over the North Atlantic present in all the CMIP6 models analysed (Figure S7). All models show too-strong SLP pressure over the North Atlantic, which advects cold air into Scandinavia and likely suppresses convection and warms the rest of Europe.

The winter bias pattern is similar to summer, with warm biases over the UK and southern Europe and cold biases over East Scandinavia, but generally with less agreement between models (Figure 4d,f). As for summer, SAT biases seem to be related to SLP biases. Figure S8 shows that all the models have too high SLP over southern Europe, which could explain the warm bias and low pressure over the Northeast Atlantic that could reduce the advection of relatively warmer Atlantic air into Scandinavia, causing the cold bias over this area.

In the next step, we analyse potential relationships between SAT signal bias and mean bias in the CMIP6 ensemble (Figure 5). In DJF, most models (10 out of 17) overestimate the warming signal in southern Europe with respect to both ERA5 and E-OBS. Consistent with Figure 4, 13 out of 17 models have a warm mean bias (Figure 5a,c). Figure 5a,c also shows that as the model SAT mean bias increases, the signal bias decreases, suggesting that climatologically warmer models tend to have smaller warming signals (Figure 5a,c). This statistical relationship is robust for biases to ERA5 ($r = -0.65$) and E-OBS ($r = -0.66$) both statistically significant at the 95% level. A similar relation is apparent for DJF in northern Europe, although much weaker ($r = -0.37$) and not statistically significant (Figure 5b,d).

The reason for this relationship is unclear. However, we explored if it could be a consequence of a relationship between warming and the expansion of the subtropical dry zones (particularly affecting southern Europe) as a response to global warming (Cresswell-Clay et al., 2022; Grise & Davis, 2020; Nguyen et al., 2015). The reasoning is that, especially in winter, when circulation changes are relatively more important than in summer (Brogli et al., 2019), the subtropical highs are located too far north in the warmer models, encroaching into south Europe. In these models, any further expansion of the subtropical highs as a response to warming would have less effect on the warming signal compared to models where expansion of a more southerly high-pressure system affects the European climate to a greater extent. Tentative evidence supporting this hypothesis is presented in Figure 6. Figure 6a shows that the models with higher mean SLP tend to have a higher mean SAT with a statistically

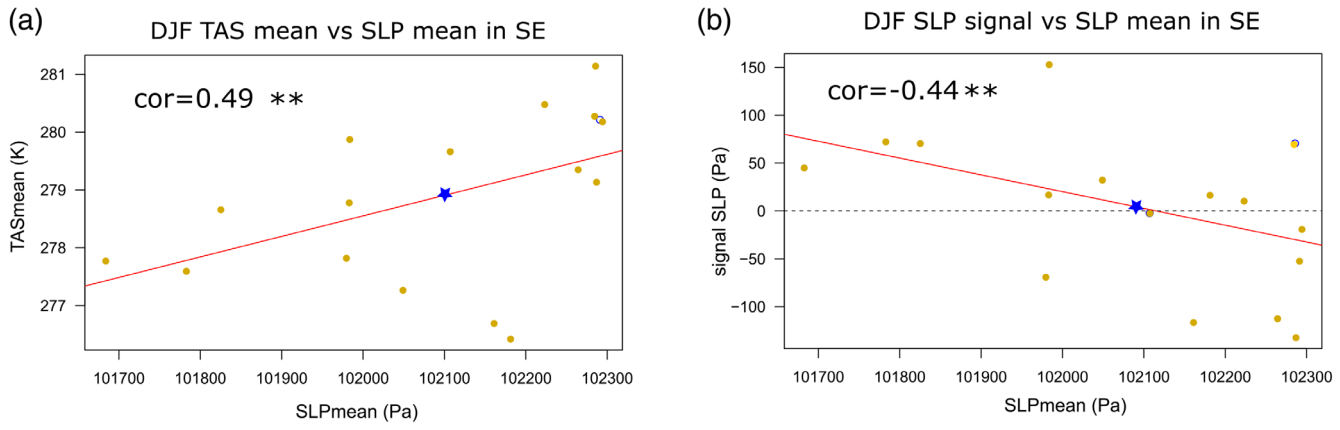

FIGURE 6 Scatter plots of CMIP6 DJF climatological SAT versus climatological SLP (a) and SLP signal versus climatological SLP (b) area-averaged over south Europe. The red line indicates the line of best fit for the scatter points shown by gold. The blue start shows the multi-model ensemble mean. The correlation coefficient of the scatter plots is shown on each panel. Asterisks (**) indicates correlations coefficients statistical significant at the 95% level [Colour figure can be viewed at wileyonlinelibrary.com]

significant correlation of $r = 0.49$. Moreover, Figure 6b shows that the models with higher mean SLP tend to have a weaker SLP signal suggesting that the models with a too-far north or stronger subtropical high tend to have a weaker subtropical high expansion. However, there is no direct relationship between the SAT signal and the SLP signal (not shown); therefore, the explanation is inconclusive. Further exploration of this hypothesis is out of the scope of this paper and will be the topic of future work.

In JJA, the signal biases in southern Europe are smaller than for winter, and all but three models have a warm mean bias (Figure 5e,f). Generally, warmer models tend to have a larger warming signal, but the correlation coefficients are small ($r = 0.25$ for ERA5 and 0.22 for E-OBS) and not statistically significant. However, MIROC6 has a very large warm bias, which exceeds 5 K using both observational datasets despite having signal biases close to the ensemble mean. Removing this model from the analysis would give a stronger correlation coefficient between the climatological and signal biases. This substantial warm bias is identified at global scales over land (Allan et al., 2022) and may be linked to a positive energy imbalance of about 1 $W \cdot m^{-2}$ in the model's pre-industrial spin-up experiment and underestimation of outgoing longwave

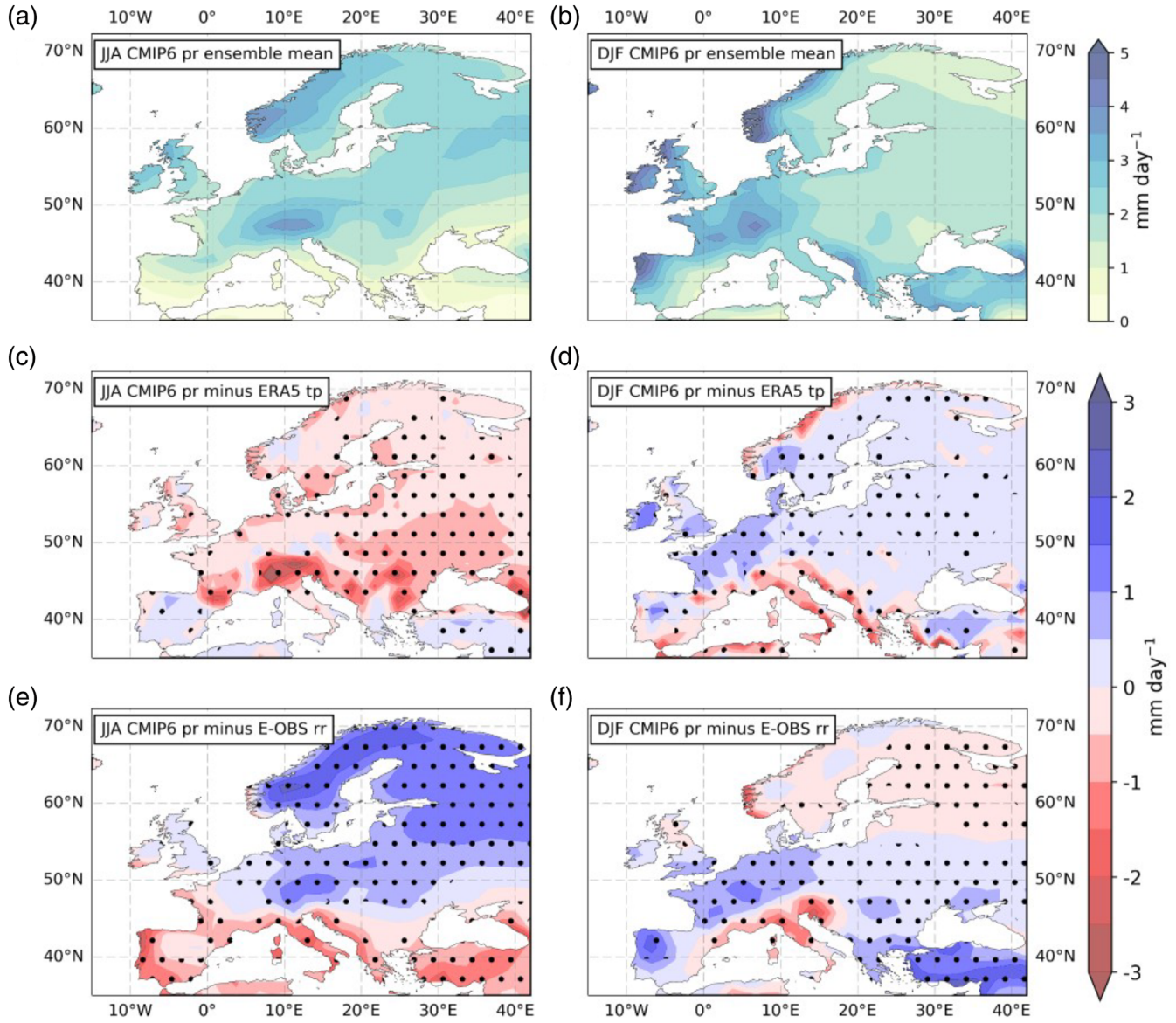

FIGURE 7 Maps of (a, b) CMIP6 ensemble climatological means for pr, (c, d) climatological biases using ERA5 tp and (e, f) climatological biases using E-OBS rr for JJA and DJF calculated across 1950–2014. The biases are calculated as model minus observations, so the blue (positive) contours indicate greater model precipitation and the red (negative) contours indicate less model precipitation. Stippling in (c–f) shows where at least two-thirds of the CMIP6 models agree on the sign of the climatological bias [Colour figure can be viewed at wileyonlinelibrary.com]

radiation (OLR) in the pre-industrial control experiment compared to observations (Tatebe et al., 2019).

Several authors showed evidence of coupling between SM and local temperatures at intraseasonal and interannual timescales (e.g., Dirmeyer, 2011; Ferranti & Viterbo, 2006; Fischer et al., 2007). At longer timescales, evidence has also shown positive feedback over Europe between SM and temperature variability (Seneviratne et al., 2006, 2010). In these studies, the projected increase in temperature variability is partially attributed to mean changes in SM (drying) over southern and central Europe. The cross-correlation analysis between the temperature signal bias and mean SM bias (Tables S1 and S2) shows no relationship between model warming biases and SM mean biases ($r = -0.13$, and not statistically significant). This suggests that the mechanisms by which SM–atmosphere interactions affect climate variability do not have the same effect on the mean climatic changes and cannot explain model differences.

4.2 | Precipitation

Figure 7 shows the CMIP6 ensemble mean PREC and the bias to ERA5 and E-OBS for JJA (left panel) and DJF (right panel). In JJA, there is a striking difference between the biases from ERA5 (Figure 7c) and the biases from E-OBS (Figure 7e). For ERA5, the CMIP6 ensemble mean has a dry bias over most continental Europe, which is especially large over the Alps and the Pyrenees.

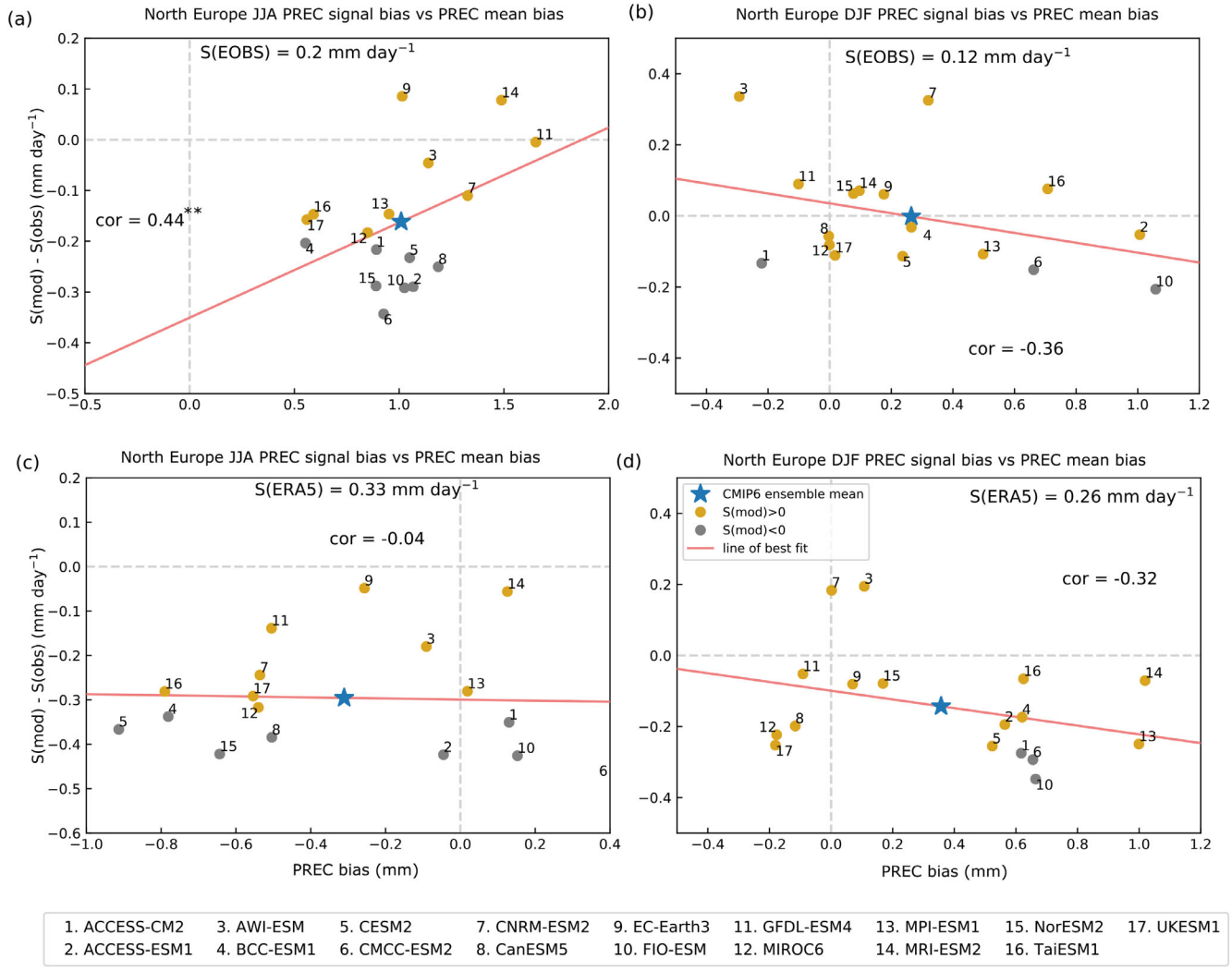

FIGURE 8 Scatter plots of area-averaged CMIP6 climatological precipitation bias and signal bias for north Europe in JJA for E-OBS (a) and ERAS (c). (b, d) Same as (a, c) but for DJF. The star indicates the climatological and signal bias for the CMIP6 ensemble mean. The red line indicates the line of best fit for the scatter points shown by gold (positive signal) or black (negative signal) circles. The correlation coefficient between the climatological and signal biases is shown on each panel along with the area-averaged signal. Asterisks (**) indicate correlation coefficients statistically significant at the 95% level [Colour figure can be viewed at wileyonlinelibrary.com]

However, for E-OBS, the models have a large wet bias over central and north Europe and Scandinavia and a dry bias over southern Europe. In DJF, the differences between the CMIP6 ERA5 (Figure 7d) and E-OBS (Figure 7f) biases are not as large as for JJA. Both show a wet bias over central and north Europe and a dry bias over the Mediterranean. However, opposite biases are apparent in Scandinavia and the Balkans.

Further insights can be obtained by the scatterplots between the PREC signal bias and mean bias shown in Figure 8. In JJA, with respect to E-OBS (Figure 8a), all models are too wet, and all but two underestimate the wetting signal (seven have a negative signal, indicating decreased PREC). The scatter plot suggests that wetter models tend to have a larger positive (or less negative) signal and a smaller signal bias with a statistically significant correlation of $r = 0.44$. However, no relationship is found when the bias is calculated with respect to ERA5 (Figure 8c). In that case, all models underestimate the signal and 11 out of the 17 models have a dry mean bias which is entirely inconsistent with the biases to E-OBS.

In DJF, an inverse relationship between signal biases and mean biases for north Europe is apparent, suggesting that the models with the strongest wet bias tend to have smaller wetting signals. The relationship holds for ERA5 and E-OBS, although the correlation coefficients are small and not statistically significant ($r = -0.36$ for E-OBS and $r = -0.32$ for ERA5) (Figure 8b,d). Four models (ACCESS-CM2, CMCC-ESM2 and FIO-ESM) have a negative signal compared to E-OBS and ERA5, although ACCESS-CM2 is climatologically drier than E-OBS. AWI-ESM and CNRM-ESM2 are notable outliers with substantial positive signal biases compared to E-OBS and ERA5, indicating that their PREC is increasing at a greater rate than the observations or reanalysis.

4.3 | Soil moisture

Figure 9 shows the CMIP6 ensemble mean SM and the bias to ERA5 for JJA (left panel) and DJF (right panel). Since there is no observational estimate, model biases

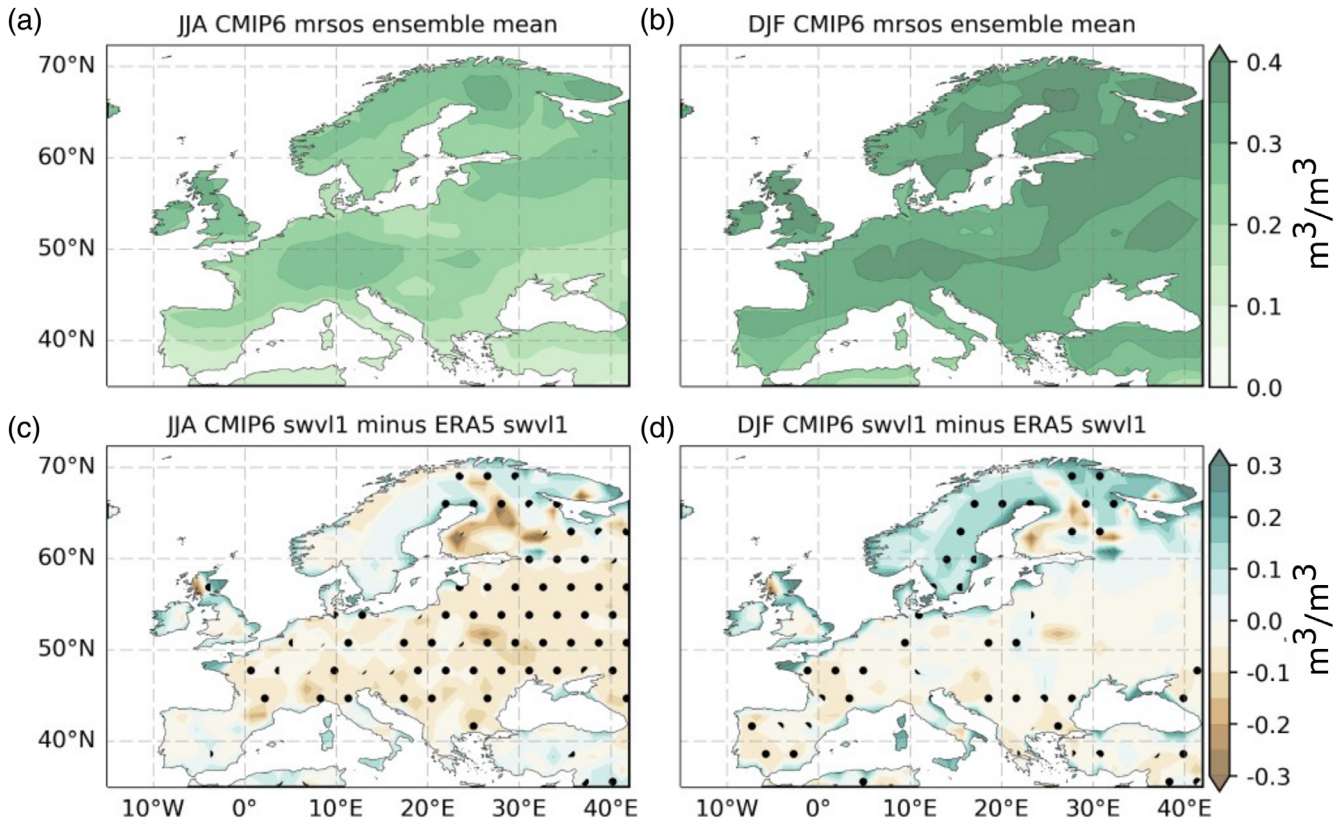

FIGURE 9 Maps of (a, b) climatological ensemble mean CMIP6 mrsos and (c, d) climatological biases using ERA5 swvl1 for JJA and DJF calculated across 1950–2014. The biases are calculated as model minus observations so the green (positive) contours indicate greater model soil moisture and brown (negative) contours indicate less model soil moisture. Stippling in (c, d) shows where at least two-thirds of the CMIP6 models agree on the sign of the climatological bias [Colour figure can be viewed at wileyonlinelibrary.com]

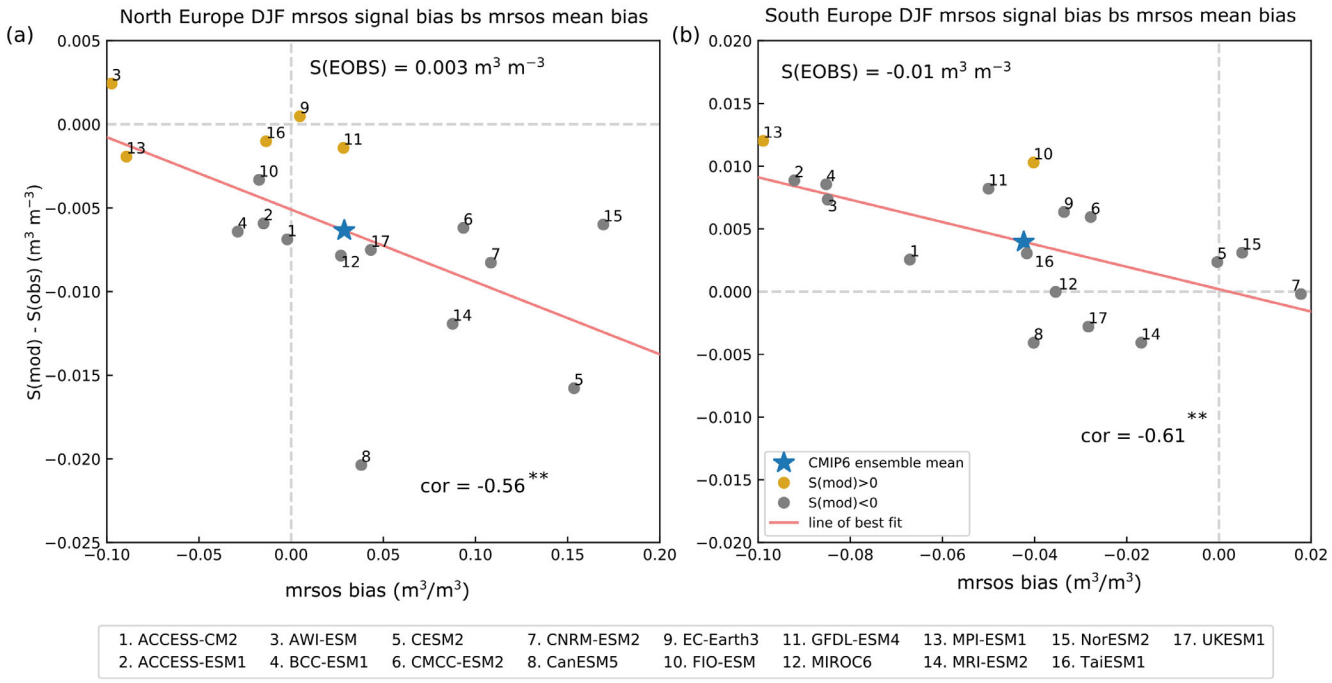

FIGURE 10 Scatter plots of area-averaged CMIP6 climatological soil moisture bias and signal bias for north Europe DJF (a) and south Europe DJF (b) for ERAS. The star indicates the climatological and signal bias for the CMIP6 ensemble mean. The red line indicates the line of best fit for the scatter points, which are shown by gold (positive signal) or black (negative signal) circles. The correlation coefficient between the climatological and signal biases is shown on each panel, along with the area-averaged ERAS signal. Asterisks (**) indicates correlation coefficients statistically significant at the 95% level [Colour figure can be viewed at wileyonlinelibrary.com]

with respect to ERA5 may also relate to deficiencies in the ERA5 model, though the input of precipitation and potential evaporative response to temperature changes are expected to be realistic. In JJA, the CMIP6 ensemble mean underestimates the SM over continental Europe, and at least 2/3 of the models agree with the sign of the bias. In winter, continental Europe biases are small, but most models have a dry bias over the Iberian Peninsula and west France and a wet bias over Norway and Sweden.

The scatter plot between the signal bias versus the mean biases of SM suggests a strong linear relationship between them in DJF, both in northern ($r = -0.56$) (Figure 10b) and southern ($r = -0.61$) Europe (Figure 10b), both statistically significant at the 95% level. The relation suggests that models with excess SM tend to dry faster. This could be a simple consequence of dry models being unable to dry further, but vegetation stomata regulation, which affects plant water use efficiency, could also play a role. In northern Europe, 10 out of 17 models have a wet soil climatological bias, and all but two models have negative signal biases (excess drying). Five out of 17 models have a positive signal (increasing SM), and the rest have a negative signal (decreasing SM). The CanESM5 model is a notable outlier with a much stronger negative signal bias and drying signal than other models. In southern Europe, 15 of the 17 models have a dry mean bias, and all but four models have positive signal biases (i.e., models dry too little or even increase soil moisture [models 10 and 13]) (Figure 10b).

5 | DISCUSSION

5.1 | Decadal and multidecadal variability

The regression scheme applied in this manuscript aims to separate the forced response from the internal variability. However, due to the relatively short span of the observational products, decadal and multidecadal variability modulating the GMST is likely to impact the results. We test the impact of internal variability in the S/N patterns by calculating the SAT signal for all members of ACCESS-ESM1-5, which has a large ensemble of 40 runs. These runs only differ from their initial conditions and have an identical representation of the physical

processes. We have performed the same test for precipitation. However, the spatial variability of the precipitation signals is very large in the models, so the average spatial signal is tiny (see Figures S3 and S4), making the interpretation of the test results meaningless. Figure S11 shows box plots of the SAT signal over southern and northern Europe for winter and summer for all the CMIP6 models (green dots) and the 40 ensemble members of ACCESS-ESM1-5 (red dots). Their corresponding standard deviation quantifies the spread. The signal spread is larger for the 16 CMIP6 models than for the 40 ACCESS members especially over southern Europe suggesting that a portion of the spread can be attributed to different model physics. However, the figures also indicate that the impact of the large-scale decadal variability is not negligible and impacts the model signals.

5.2 | Aerosol external forcing

Anthropogenic aerosols have been the second dominant driver of forced climate change after GHGs and have an opposite radiative impact (Myhre et al., 2013). Sulphate aerosols directly influence the Earth's radiative budget by scattering shortwave radiation and indirectly by changing the clouds' albedo, lifetime and precipitation efficiency (e.g., Bellouin et al., 2020). The total aerosol radiative forcing in 2011 with respect to pre-industrial times is assessed to be -0.45 ± 0.5 W·m^{-2}, and aerosol-cloud interaction estimated as -0.45 [-1.2 to 0.0] W·m^{-2} (Gulev et al., 2021 IPCC AR6, Chapter 2). Globally, the aerosol optical depth increased from pre-industrial times up to 1990, slowly decreasing afterwards. Since aerosols have the opposite impact on the GMST than GHGs (Forster et al., 2021), their effect is included in the term $L(t)$ (see Equation (1)). The early period of our analysis (~1950–1983) was a relatively cool period due to anthropogenic aerosol (e.g., Wang & Wen, 2022), and therefore the magnitude of the signals is potentially amplified in our calculations. Furthermore, since aerosol radiative forcing is more uncertain than GHGs (Forster et al., 2021) this contributes to an additional spread in the model simulated signal of climate change as the spatial pattern and magnitude of aerosol forcing changes over time (Forster et al., 2021).

Another potential influence in the signals is volcanic eruptions. Explosive volcanic eruptions can affect the global climate by injecting large quantities of aerosols (especially sulphur compounds) into the stratosphere (e.g., Hansen et al., 1997). The aerosols tend to cool the surface, warm the stratosphere and, in some instances, modify the meridional temperature gradients and the tropospheric circulation patterns (e.g., Robock, 2000). However, the *e*-folding residence time of aerosols in the stratosphere is about 1 year and only two major eruptions, the 1963 Agung eruption and the 1982 El Chichon, occurred in our baseline period. Moreover, no major eruption occurred at the end of the analysed period, so the direct impact of volcanism in the signals should be small overall. However, there is evidence that volcanism as well as anthropogenic aerosol could also impact the climate at the decadal time scale by forcing changes in oceanic modes of variability such as the ENSO or the AMOC (e.g., Ding et al., 2014; Hermanson et al., 2020; Iwi et al., 2012; Menary et al., 2020) which likely affect our results.

5.3 | Emergent constraints

An emergent constraint is a relationship between the intermodel spread of the climate change response of some variable to present-day biases or short-term variations that can be observed (e.g., Brient, 2020). These relations can potentially be used to constrain the future response in climate projections. In this work, we have analysed the relationships between the models signals and their climatological biases and found a relationship in southern Europe between SAT signal biases and SAT mean biases, suggesting that the climatologically too-warm models tend to warm less. Several conditions/uncertainties must be considered when evaluating the robustness of an emergent constraint: (1) An emergent constraint must be supported with a physical understanding of the mechanisms underlying the statistical relationship. (2) The observational period must be long enough, and the uncertainty of the observations small enough so that not all the models are consistent with the observations. (3) The emergent constraint inference method treats the model set as a random sample, but models share components and often derive from each other (Knutti et al., 2013). These limitations must be taken into account when evaluating the emergent constraint robustness.

We have proposed that the reported relationship for SAT in southern Europe could be related to the position of the subtropical highs, and we have found the same relationship for two observational datasets (E-OBS and ERA5). However, the physical hypothesis requires further analysis and the set of CMIP6 models used is relatively small. To consider the reported relationship an emergent constraint and use it to constrain future SAT projections would require analysing an extended model set and further quantifying observational uncertainty. Furthermore, as proposed by Hall et al. (2019) to verify that the statistical relationship has not been found by chance, the same relationship should also be found in sensitivity experiments in which a range of climatological SAT are imposed in a model. Overall, we consider that the reported

relationship merits further inquiry and its potential as emergent constrain will be the topic of future research.

6 | SUMMARY

In this manuscript, we have assessed the emergence of climate change signals in CMIP6 during the 1950–2014 period over Europe, compared these with observations and investigated the reasons for discrepancies. Climate change signals are evaluated from the signal-to-noise ratio (S/N) of three variables with a significant societal impact: surface air temperature (SAT) and precipitation (PREC), which are evaluated against ERA5 and E-OBS, and soil moisture (SM) which is compared solely against ERA5 due to the lack of dense SM observational networks. In the following, we summarize the main results.

6.1 | Temperature climate change signals

In JJA, the CMIP6 multimodel ensemble mean SAT S/N is larger than one across the entire domain, indicating that during the last decade, all of Europe experienced "unusual" SAT compared to the mid-XX century. The pattern and magnitude of the CMIP6 ensemble mean S/N are similar to ERA5. In contrast, E-OBS has generally smaller S/N values, especially in eastern Europe, Scandinavia and the UK. An analysis of the individual models shows that all agree on the warming signal positive sign, although the warming magnitude varies among models. The magnitude of the discrepancy is especially large over western Europe, UK and Scandinavia and smaller over eastern Europe. An analysis of the models SLP signals reveals a large range of circulation responses involving different advection patterns, which could partially explain the differences in the SAT signals (Figures S10 and S11).

Biases in the SLP patterns also seem to be associated with the models SAT mean biases. Most models have a warm bias in southern Europe and a cold bias in northern Europe which appears to be related to a too-strong SLP pressure over the North Atlantic, which advects cold air towards Scandinavia and likely suppresses convection and warms the rest of Europe.

We also analyse whether model differences in SM are related to their SAT differences. Interestingly, we found no relation between models SM bias and their SAT signals; drier models do not generally warm faster. This suggests that the mechanisms by which SM-atmosphere interactions affect climate variability did not have the same effect on the mean climatic changes during the studied period and cannot explain model differences.

In DJF, there is a good agreement between the CMIP6 ensemble mean SAT S/N and the S/N from ERA5 and E-OBS. The S/N spread among CMIP6 models is similar to summer but relatively much larger when compared to DJF S/N values. In particular, five models show extensive cooling areas, clearly at odds with observations. We found evidence that these intermodel discrepancies could be related to differences in the models mean biases. In particular, we have found a robust relationship in southern Europe between SAT signal biases and SAT mean biases, suggesting that the climatologically too warm models tend to warm less. Tentative evidence suggests that this could be related to the position of the subtropical highs (see section 5).

6.2 | Precipitation climate change signals

The CMIP6 ensemble mean does not show any significant change in PREC in all the domain during summer or winter ($|S/N| < 0.5$) for the 1950–2014 period. In JJA, the CMIP6 ensemble S/N pattern is strikingly different from ERA5 and E-OBS, which show a SW–NE diagonal divide with decreasing PREC to the south and increased PREC to the north. An analysis of the individual model patterns shows that these discrepancies are due to the large diversity of S PREC patterns among models, with several showing opposite patterns. For example, 7 of the 18 models analysed show an overall increase in southern Europe PREC, which is clearly at odds with observations. This result suggests that the PREC S/N ensemble mean does not represent the forced response well.

In DJF, the ensemble mean S/N pattern indicates an increase in PREC over most of Europe except south Iberia and some small regions of the Mediterranean coast. This pattern resembles that of the E-OBS but is remarkably different from ERA5, which exhibits a clear SW–NE divide with increased PREC to the north and a decrease to the south. The difference between models and ERA5 could be attributed to a too-zonal North Atlantic jet stream in the models, resulting in the jet intercepting the European continent too far south.

Both in DJF and JJA, the SLP S/N patterns for individual models correlated well with their PREC S/N, suggesting that the intermodal differences in the PREC signals can be attributed to divergent circulation changes as a response to global warming together with the mean jet stream bias.

6.3 | Soil moisture climate change signals

In summer, the CMIP6 ensemble mean S/N indicates that the SM has decreased over all of Europe, although the S/N has not crossed the threshold for an "unusual" climate ($|S/N| > 1$). ERA5 also shows a decrease in SM over most of Europe except Southern Scandinavia, the UK and Ireland. The S/N is smaller than −1 (signifying unusual soil drying) over some areas of Spain, the Alps and Scandinavia and larger than +1 (unusually wet) in Ireland. Despite the broad agreement between the CMIP6 ensemble mean and the observations, the individual models S/N response is very diverse, sometimes showing opposite patterns. Over continental Europe, the models SM S/N closely follow their S/N PREC pattern. However, this is not the case in Scandinavia, where some models show a PREC increase but soil drying, which could be linked to a reduced/early snowmelt in spring (e.g., Manabe et al., 1981; Mitchell & Warrilow, 1987; Ruosteenoja et al., 2018).

In winter, the CMIP6 ensemble mean S/N indicates a decrease in SM over most of Europe except over some areas of Scandinavia. This pattern differs from ERA5, which shows a SW–NE diagonal divide with an increase of SM to the north and a decrease to the south, which resembles its S/N PREC pattern. The diversity in the climate change signals of SM among individual models is striking, with many models showing opposite patterns. Interestingly, several models show a decoupling between the SM and PREC signals, with extensive SM decreases despite increased PREC.

The relationship between soil-moisture signal biases and mean biases shows that in winter, both in the north and southern Europe, the models with excess SM tend to dry faster. This could be a simple consequence of dry models being unable to dry further and perhaps with the vegetation stomata regulation with models with no SM limitation increasing evapotranspiration.

Finally, a key message from this work is also that the emergence of climate change signals, even for temperature, is affected by data coverage. This is evidenced by the remarkably different S/N temperature and PREC patterns between ERA5 and E-OBS. This pattern diversity in the observations complicates the evaluation of climate models at the regional scale and highlights the critical importance of creating and maintaining high-quality, dense observational networks.

AUTHOR CONTRIBUTIONS

Albert Ossó: Conceptualization; investigation; writing – original draft; methodology; formal analysis. **Philip Craig:** Writing – original draft; writing – review and editing; investigation; formal analysis; data curation; conceptualization. **Richard P. Allan:** Writing – review and editing; conceptualization; supervision; investigation.

ACKNOWLEDGEMENTS

This work was funded by the INDECIS Project, which is part of ERA4CS, an ERA-NET initiated by JPI Climate, and funded by FORMAS (SE), DLR (DE), BMWFW (AT), IFD (DK), MINECO (ES), ANR (FR) with co-funding by the European Union (Grant 690462). Funding for Open access is provided by the University of Graz.

ORCID

Albert Ossó https://orcid.org/0000-0001-5653-4886
Philip Craig https://orcid.org/0000-0001-9213-4599
Richard P. Allan https://orcid.org/0000-0003-0264-9447

REFERENCES

Allan, R.P., Willett, K.M., John, V.O. & Trent, T. (2022) Global changes in water vapor 1979–2020. *Journal of Geophysical Research: Atmospheres*, 127, e2022JD036728. Available from: https://doi.org/10.1029/2022JD036728

Bao, Y., Song, Z. & Qiao, F. (2020) FIO-ESM version 2.0: model description and evaluation. *Journal of Geophysical Research: Oceans*, 125, e2019JC016036. Available from: https://doi.org/10.1029/2019JC016036

Bell, B., Hersbach, H., Simmons, A., Berrisford, P., Dahlgren, P., Horányi, A. et al. (2021) The ERA5 global reanalysis: preliminary extension to 1950. *Quarterly Journal of the Royal Meteorological Society*, 147(741), 4186–4227. Available from: https://doi.org/10.1002/qj.4174

Bellouin, N., Quaas, J., Gryspeerdt, E., Kinne, S., Stier, P., Watson-Parris, D. et al. (2020) Bounding global aerosol radiative forcing of climate change. *Reviews of Geophysics*, 58, e2019RG000660. Available from: https://doi.org/10.1029/2019RG000660

Bi, D., Dix, M., Marsland, S., O'farrell, S., Sullivan, A., Bodman, R. et al. (2020) Configuration and spin-up of ACCESS-CM2, the new generation Australian community climate and earth system simulator coupled model. *Journal of Southern Hemisphere Earth Systems Science*, 70(1), 225–251. Available from: https://doi.org/10.1071/ES19040

Brient, F. (2020) Reducing uncertainties in climate projections with emergent constraints: concepts, examples and prospects. *Advances in Atmospheric Sciences*, 37, 1–15. Available from: https://doi.org/10.1007/s00376-019-9140-8

Brogli, R., Sørland, S.L., Kröner, N. & Schär, C. (2019) Causes of future Mediterranean precipitation decline depend on the season. *Environmental Research Letters*, 14(11), 114017. Available from: https://doi.org/10.1088/1748-9326/ab4438

Carvalho, D., Cardoso Pereira, S. & Rocha, A. (2021) Future surface temperatures over Europe according to CMIP6 climate projections: an analysis with original and bias-corrected data. *Climatic Change*, 167, 10. Available from: https://doi.org/10.1007/s10584-021-03159-0

Cattiaux, J., Douville, H. & Peings, Y. (2013) European temperatures in CMIP5: origins of present-day biases and future

uncertainties. *Climate Dynamics*, 41, 2889–2907. Available from: https://doi.org/10.1007/s00382-013-1731-y

Ceglar, A., Croitoru, A.E., Cuxart, J., Djurdjevic, V., Güttler, I., Ivančan-Picek, B. et al. (2018) PannEx: the pannonian basin experiment. *Climate Services*, 11, 78–85. Available from: https://doi.org/10.1016/j.cliser.2018.05.002

Cherchi, A., Fogli, P.G., Lovato, T., Peano, D., Iovino, D., Gualdi, S. et al. (2019) Global mean climate and main patterns of variability in the CMCC-CM2 coupled model. *Journal of Advances in Modeling Earth Systems*, 11, 185–209. Available from: https://doi.org/10.1029/2018MS001369

Collins, M., Knutti, R., Arblaster, J., Dufresne, J.-L., Fichefet, T., Friedlingstein, P. et al. (2013) Long-term climate change: projections, commitments and irreversibility. In: *Climate change 2013: the physical science basis. IPCC working group I contribution to AR5*. Cambridge: Cambridge University Press.

Cornes, R.C., van der Schrier, G., van den Besselaar, E.J.M. & Jones, P.D. (2018) An ensemble version of the E-OBS temperature and precipitation data sets. *Journal of Geophysical Research: Atmospheres*, 123, 9391–9409. Available from: https://doi.org/10.1029/2017JD028200

Craig, P.M. & Allan, R.P. (2022) The role of teleconnection patterns in the variability and trends of growing season indices across Europe. *International Journal of Climatology*, 42(2), 1072–1091. Available from: https://doi.org/10.1002/joc.7290

Cresswell-Clay, N., Ummenhofer, C.C., Thatcher, D.L., Wanamaker, A.D., Denniston, R.F., Asmerom, Y. et al. (2022) Twentieth-century Azores High expansion unprecedented in the past 1,200 years. *Nature Geoscience*, 15, 548–553. Available from: https://doi.org/10.1038/s41561-022-00971-w

Danabasoglu, G., Lamarque, J.-F., Bacmeister, J., Bailey, D.A., DuVivier, A.K., Edwards, J. et al. (2020) The Community Earth System Model Version 2 (CESM2). *Journal of Advances in Modeling Earth Systems*, 12, e2019MS001916. Available from: https://doi.org/10.1029/2019MS001916

Deser, C. (2020) Certain uncertainty: the role of internal climate variability in projections of regional climate change and risk management. *Earth's Future*, 8, e2020EF001854. Available from: https://doi.org/10.1029/2020EF001854

Diffenbaugh, N.S., Pal, J.S., Giorgi, F. & Gao, X. (2007) Heat stress intensification in the Mediterranean climate change hotspot. *Geophysical Research Letters*, 34, L11706. Available from: https://doi.org/10.1029/2007GL030000

Ding, Y., Carton, J.A., Chepurin, G.A., Stenchikov, G., Robock, A., Sentman, L.T. et al. (2014) Ocean response to volcanic eruptions in Coupled Model Intercomparison Project 5 simulations. *Journal of Geophysical Research: Oceans*, 119, 5622–5637. Available from: https://doi.org/10.1002/2013JC009780

Dirmeyer, P.A. (2011) The terrestrial segment of soil moisture–climate coupling. *Geophysical Research Letters*, 38, L16702. Available from: https://doi.org/10.1029/2011GL048268

Doblas, R., Déqué, F.J., Valero, F. & Stephenson, D.B. (1998) North Atlantic wintertime intraseasonal variability and its sensitivity to GCM horizontal resolution. *Tellus A*, 50, 573–595. Available from: https://doi.org/10.1034/j.1600-0870.1998.t01-4-00002.x

Döscher, R., Acosta, M., Alessandri, A., Anthoni, P., Arneth, A., Arsouze, T. et al. (2021) The EC-earth3 Earth system model for the Climate Model Intercomparison Project 6. *Geoscientific Model Development*, 15, 2973–3020. Available from: https://doi.org/10.5194/gmd-15-2973-2022

Douville, H., Raghavan, K., Renwick, J., Allan, R.P., Arias, P.A., Barlow, M. et al. (2021) Water cycle changes. In: *Climate change 2021: the physical science basis. Contribution of working group i to the sixth assessment report of the intergovernmental panel on climate change*. Cambridge: Cambridge University Press. pp. 1055–1210. Available from: https://doi.org/10.1017/9781009157896.010

Dunne, J.P., Horowitz, L.W., Adcroft, A.J., Ginoux, P., Held, I.M., John, J.G. et al. (2020) The GFDL Earth System Model Version 4.1 (GFDL-ESM 4.1): overall coupled model description and simulation characteristics. *Journal of Advances in Modeling Earth Systems*, 12, e2019MS002015. Available from: https://doi.org/10.1029/2019MS002015

Eyring, V., Bony, S., Meehl, G.A., Senior, C.A., Stevens, B., Stouffer, R.J. et al. (2016) Overview of the Coupled Model Intercomparison Project Phase 6 (CMIP6) experimental design and organisation. *Geoscientific Model Development*, 9(5), 1937–1958. Available from: https://doi.org/10.5194/gmd-9-1937-2016

Ferranti, L. & Viterbo, P. (2006) The European summer of 2003: sensitivity to soil water initial conditions. *Journal of Climate*, 19(15), 3659–3680. Available from: https://doi.org/10.1175/JCLI3810.1

Fischer, E.M. & Knutti, R. (2014) Detection of spatially aggregated changes in temperature and precipitation extremes. *Geophysical Research Letters*, 41, 547–554. Available from: https://doi.org/10.1002/2013GL058499

Fischer, E.M., Seneviratne, S.I., Vidale, P.L., Lüthi, D. & Schär, C. (2007) Soil moisture–atmosphere interactions during the 2003 European summer heat wave. *Journal of Climate*, 20, 5081–5099. Available from: https://doi.org/10.1175/JCLI4288.1

Foley, A.M. (2010) Uncertainty in regional climate modelling: a review. *Progress in Physical Geography: Earth and Environment*, 34(5), 647–670. Available from: https://doi.org/10.1177/0309133310375654

Forster, P., Storelvmo, T., Armour, K., Collins, W., Dufresne, J.-L., Frame, D. et al. (2021) The earth's energy budget, climate feedbacks, and climate sensitivity. In: Masson-Delmotte, V., Zhai, P., Pirani, A., Connors, S.L., Péan, C., Berger, S. et al. (Eds.) *Climate change 2021: the physical science basis. Contribution of working group I to the sixth assessment report of the Intergovernmental Panel on Climate Change*. Cambridge and New York, NY: Cambridge University Press, pp. 923–1054. Available from: https://doi.org/10.1017/9781009157896.009

Frame, D., Joshi, M., Hawkins, E., Harrington, L.J. & de Roiste, M. (2017) Population-based emergence of unfamiliar climates. *Nature Climatic Change*, 7, 407–411. Available from: https://doi.org/10.1038/nclimate3297

Frieler, K., Meinshausen, M., Mengel, M., Braun, N. & Hare, W. (2012) A scaling approach to probabilistic assessment of regional climate change. *Journal of Climate*, 25(9), 3117–3144.

Giorgi, F. & Coppola, E. (2010) Does the model regional bias affect the projected regional climate change? An analysis of global model projections. *Climatic Change*, 100, 787–795. Available from: https://doi.org/10.1007/s10584-010-9864-z

Giorgi, F. & Francisco, R. (2000) Evaluating uncertainties in the prediction of regional climate change. *Geophysical Research*

Letters, 27(9), 1295–1298. Available from: https://doi.org/10.1029/1999GL011016

Grise, K.M. & Davis, S.M. (2020) Hadley cell expansion in CMIP6 models. *Atmospheric Chemistry and Physics*, 20(9), 5249–5268. Available from: https://doi.org/10.5194/acp-20-5249-2020

Gulev, S.K., Thorne, P.W., Ahn, J., Dentener, F.J., Domingues, C. M., Gerland, S. et al. (2021) Changing state of the climate system. In: *Climate change 2021: the physical science basis. Contribution of working group i to the sixth assessment report of the intergovernmental panel on climate change*. Cambridge: Cambridge University Press. pp. 287–422. Available from: https://doi.org/10.1017/9781009157896.004

Gutiérrez, J.M., Jones, R.G., Narisma, G.T., Alves, L.M., Amjad, M., Gorodetskaya, I.V. et al. (2021) Atlas. In: *Climate change 2021: the physical science basis. Contribution of working group i to the sixth assessment report of the intergovernmental panel on climate change*. Cambridge: Cambridge University Press. pp. 1927–2058. Available from: https://doi.org/10.1017/9781009157896.021

Hall, A., Cox, P., Huntingford, C. & Klein, S. (2019) Progressing emergent constraints on future climate change. *Nature Climate Change*, 9, 269–278. Available from: https://doi.org/10.1038/s41558-019-0436-6

Hansen, J., Sato, M., Lacis, A. & Ruedy, R. (1997) The missing climate forcing. *Philosophical Transactions of the Royal Society of London. Series B: Biological Sciences*, 352(1350), 231–240.

Hawkins, E., Frame, D., Harrington, L., Joshi, M., King, A., Rojas, M. et al. (2020) Observed emergence of the climate change signal: from the familiar to the unknown. *Geophysical Research Letters*, 47, e2019GL086259. Available from: https://doi.org/10.1029/2019GL086259

Hawkins, E. & Sutton, R. (2009) The potential to narrow uncertainty in regional climate predictions. *The Bulletin of the American Meteorological Society*, 90, 1095–1108. Available from: https://doi.org/10.1175/2009BAMS2607.1

Hawkins, E. & Sutton, R. (2012) Time of emergence of climate signals. *Geophysical Research Letters*, 39, L01702. Available from: https://doi.org/10.1029/2011GL050087

Hermanson, L., Bilbao, R., Dunstone, N., Ménégoz, M., Ortega, P., Pohlmann, H. et al. (2020) Robust multiyear climate impacts of volcanic eruptions in decadal prediction systems. *Journal of Geophysical Research: Atmospheres*, 125(9), e2019JD031739.

Hersbach, H., Bell, B., Berrisford, P., Hirahara, S., Horányi, A., Muñoz-Sabater, J. et al. (2020) The ERA5 global reanalysis. *Quarterly Journal of the Royal Meteorological Society*, 146, 1999–2049. Available from: https://doi.org/10.1002/qj.3803

Iwi, A.M., Hermanson, L., Haines, K. & Sutton, R.T. (2012) Mechanisms linking volcanic aerosols to the Atlantic meridional overturning circulation. *Journal of Climate*, 25(8), 3039–3051. Available from: https://doi.org/10.1175/2011JCLI4067.1

Jasper, K., Calanca, P., Gyalistras, D. & Fuhrer, J. (2004) Differential impacts of climate change on the hydrology of two alpine river basins. *Climate Research*, 26(2), 113–129. Available from: https://doi.org/10.3354/cr026113

Knutti, R., Masson, D. & Gettelman, A. (2013) Climate model genealogy: generation CMIP5 and how we got there. *Geophysical Research Letters*, 40(6), 1194–1199.

Lopez, A., Suckling, E.B. & Smith, L.A. (2014) Robustness of pattern scaled climate change scenarios for adaptation decision support. *Climatic Change*, 122, 555–566.

Manabe, S., Wetherald, R.T. & Stouffer, R.J. (1981) Summer dryness due to an increase of atmospheric CO_2 concentration. *Climatic Change*, 3, 347–386. Available from: https://doi.org/10.1007/BF00139743

Maraun, D. (2013) When will trends in European mean and heavy daily precipitation emerge? *Environmental Research Letters*, 8, 14004. Available from: https://doi.org/10.1088/1748-9326/8/1/014004

Marty, C. & Meister, R. (2012) Long-term snow and weather observations at Weissfluhjoch and its relation to other high-altitude observatories in the Alps. *Theoretical and Applied Climatology*, 110, 573–583. Available from: https://doi.org/10.1007/s00704-012-0584-3

Mauritsen, T., Bader, J., Becker, T., Behrens, J., Bittner, M., Brokopf, R. et al. (2019) Developments in the MPI-M Earth System Model version 1.2 (MPI-ESM1.2) and its response to increasing CO_2. *Journal of Advances in Modeling Earth Systems*, 11, 998–1038. Available from: https://doi.org/10.1029/2018MS001400

Meehl, G.A., Senior, C.A., Eyring, V., Flato, G., Lamarque, J.-F., Stouffer, R.J. et al. (2020) Context for interpreting equilibrium climate sensitivity and transient climate response from the CMIP6 Earth system models. *Science Advances*, 6, eaba1981. Available from: https://doi.org/10.1126/sciadv.aba1981

Menary, M.B., Robson, J., Allan, R.P., Booth, B.B.B., Cassou, C., Gastineau, G. et al. (2020) Aerosol-forced AMOC changes in CMIP6 historical simulations. *Geophysical Research Letters*, 47, e2020GL088166. Available from: https://doi.org/10.1029/2020GL088166

Mitchell, J. & Warrilow, D. (1987) Summer dryness in northern mid-latitudes due to increased CO_2. *Nature*, 330, 238–240. Available from: https://doi.org/10.1038/330238a0

Morice, C.P., Kennedy, J.J., Rayner, N.A., Winn, J.P., Hogan, E., Killick, R.E. et al. (2021) An updated assessment of near-surface temperature change from 1850: the HadCRUT5 data set. *Journal of Geophysical Research: Atmospheres*, 126, e2019JD032361. Available from: https://doi.org/10.1029/2019JD032361

Myhre, G., Myhre, C.E.L., Samset, B.H. & Storelvmo, T. (2013) Aerosols and their relation to global climate and climate sensitivity. *Nature Education Knowledge*, 4(5), 7.

Nguyen, H., Lucas, C., Evans, A., Timbal, B. & Hanson, L. (2015) Expansion of the Southern Hemisphere Hadley cell in response to greenhouse gas forcing. *Journal of Climate*, 28(20), 8067–8077. Available from: https://doi.org/10.1175/JCLI-D-15-0139.1

Ohmura, A. (2012) Enhanced temperature variability in high-altitude climate change. *Theoretical and Applied Climatology*, 110, 499–508. Available from: https://doi.org/10.1007/s00704-012-0687-x

Ossó, A., Allan, R.P., Hawkins, E., Shaffrey, L. & Maraun, D. (2022) Emerging new climate extremes over Europe. *Climate Dynamics*, 58, 487–501. Available from: https://doi.org/10.1007/s00382-021-05917-3

Prein, A.F. & Gobiet, A. (2017) Impacts of uncertainties in European gridded precipitation observations on regional climate analysis. *International Journal of Climatology*, 37, 305–327. Available from: https://doi.org/10.1002/joc.4706

Robock, A. (2000) Volcanic eruptions and climate. *Reviews of Geophysics*, 38(2), 191–219.

Ruosteenoja, K., Markkanen, T., Venäläinen, A., Räisänen, P. & Peltola, H. (2018) Seasonal soil moisture and drought occurrence in Europe in CMIP5 projections for the 21st century. *Climate Dynamics*, 50, 1177–1192. Available from: https://doi.org/10.1007/s00382-017-3671-4

Santer, B.D., Po-Chedley, S., Mears, C., Fyfe, J.C., Gillett, N., Fu, Q. et al. (2021) Using climate model simulations to constrain observations. *The Journal of Climate*, 34, 6281–6301. Available from: https://doi.org/10.1175/JCLI-D-20-0768.1

Santer, B.D., Wigley, T.M.L., Schlesinger, M.E. & Mitchell, J.F.B. (1990) *Developing climate scenarios from equilibrium GCM results*. Hamburg: MPI. Report number 47.

Séférian, R., Nabat, P., Michou, M., Saint-Martin, D., Voldoire, A., Colin, J. et al. (2019) Evaluation of CNRM Earth-System model, CNRM-ESM2-1: role of Earth system processes in present-day and future climate. *Journal of Advances in Modeling Earth Systems*, 11, 4182–4227. Available from: https://doi.org/10.1029/2019MS001791

Seland, Ø., Bentsen, M., Olivié, D., Toniazzo, T., Gjermundsen, A., Graff, L.S. et al. (2020) Overview of the Norwegian Earth System Model (NorESM2) and key climate response of CMIP6 DECK, historical, and scenario simulations. *Geoscientific Model Development*, 13(12), 6165–6200. Available from: https://doi.org/10.5194/gmd-13-6165-2020

Sellar, A.A., Walton, J., Jones, C.G., Wood, R., Abraham, N.L., Andrejczuk, M. et al. (2020) Implementation of UK Earth system models for CMIP6. *Journal of Advances in Modeling Earth Systems*, 12, e2019MS001946. Available from: https://doi.org/10.1029/2019MS001946

Semmler, T., Danilov, S., Gierz, P., Goessling, H.F., Hegewald, J., Hinrichs, C. et al. (2020) Simulations for CMIP6 with the AWI climate model AWI-CM-1-1. *Journal of Advances in Modeling Earth Systems*, 12, e2019MS002009. Available from: https://doi.org/10.1029/2019MS002009

Seneviratne, S., Lüthi, D., Litschi, M. & Schär, C. (2006) Land–atmosphere coupling and climate change in Europe. *Nature*, 443, 205–209. Available from: https://doi.org/10.1038/nature05095

Seneviratne, S.I., Corti, T., Davin, E.L., Hirschi, M., Jaeger, E.B., Lehner, I. et al. (2010) Investigating soil moisture–climate interactions in a changing climate: a review. *Earth-Science Reviews*, 99(3–4), 125–161. Available from: https://doi.org/10.1016/j.earscirev.2010.02.004

Shepherd, T. (2014) Atmospheric circulation as a source of uncertainty in climate change projections. *Nature Geoscience*, 7, 703–708. Available from: https://doi.org/10.1038/ngeo2253

Simpson, I.R., Bacmeister, J., Neale, R.B., Hannay, C., Gettelman, A., Garcia, R.R. et al. (2020) An evaluation of the large-scale atmospheric circulation and its variability in CESM2 and other CMIP models. *Journal of Geophysical Research: Atmospheres*, 125, e2020JD032835. Available from: https://doi.org/10.1029/2020JD032835

Sutton, R., Suckling, E. & Hawkins, E. (2015) What does global mean temperature tell us about local climate? *Philosophical Transactions of the Royal Society A: Mathematical Physical and Engineering Sciences*, 373(2054), 20140426. Available from: https://doi.org/10.1098/rsta.2014.0426

Swart, N.C., Cole, J.N., Kharin, V.V., Lazare, M., Scinocca, J.F., Gillett, N.P. et al. (2019) The Canadian earth system model version 5 (CanESM5.0.3). *Geoscientific Model Development*, 12(11), 4823–4873. Available from: https://doi.org/10.5194/gmd-12-4823-2019

Tatebe, H., Ogura, T., Nitta, T., Komuro, Y., Ogochi, K., Takemura, T. et al. (2019) Description and basic evaluation of simulated mean state, internal variability, and climate sensitivity in MIROC6. *Geoscientific Model Development*, 12(7), 2727–2765. Available from: https://doi.org/10.5194/gmd-12-2727-2019

van den Besselaar, A.M.G., Tank, K. & Buishand, T.A. (2013) Trends in European precipitation extremes over 1951–2010. *International Journal of Climatology*, 33(12), 2682–2689. Available from: https://doi.org/10.1002/joc.3619

van der Schrier, G., van den Besselaar, E.J.M., Klein Tank, A.M.G. & Verver, G. (2013) Monitoring European average temperature based on the E-OBS gridded data set. *Journal of Geophysical Research: Atmospheres*, 118, 5120–5135. Available from: https://doi.org/10.1002/jgrd.50444

Wald, A. (1943) Tests of statistical hypotheses concerning several parameters when the number of observations is large. *Transactions of the American Mathematical Society*, 54(3), 426–482. Available from: https://doi.org/10.2307/1990256

Wang, H. & Wen, Y.J. (2022) Climate response to the spatial and temporal evolutions of anthropogenic aerosol forcing. *Climate Dynamics*, 59, 1579–1595. Available from: https://doi.org/10.1007/s00382-021-06059-2

Wang, Y.-C., Hsu, H.-H., Chen, C.-A., Tseng, W.-L., Hsu, P.-C., Lin, C.-W. et al. (2021) Performance of the Taiwan Earth System Model in simulating climate variability compared with observations and CMIP6 model simulations. *Journal of Advances in Modeling Earth Systems*, 13, e2020MS002353. Available from: https://doi.org/10.1029/2020MS002353

Watterson, I.G. (2019) Indices of climate change based on patterns from CMIP5 models, and the range of projections. *Climate Dynamics*, 52, 2451–2466. Available from: https://doi.org/10.1007/s00382-018-4260-x

Watterson, I.G. & Whetton, P.H. (2013) Probabilistic projections of regional temperature and precipitation extending from observed time series. *Climatic Change*, 119, 677–691. Available from: https://doi.org/10.1007/s10584-013-0755-y

Woollings, T. (2010) Dynamical influences on European climate: an uncertain future. *Philosophical Transactions of the Royal Society A*, 368, 3733–3756. Available from: https://doi.org/10.1098/rsta.2010.0040

Wu, T., Zhang, F., Zhang, J., Jie, W., Zhang, Y., Wu, F. et al. (2020) Beijing Climate Center Earth System Model version 1 (BCC-ESM1): model description and evaluation of aerosol simulations. *Geoscientific Model Development*, 13(3), 977–1005. Available from: https://doi.org/10.5194/gmd-13-977-2020

Yuan, S., Quiring, S.M. & Leasor, Z.T. (2021) Historical changes in surface soil moisture over the contiguous United States: an

assessment of CMIP6. *Geophysical Research Letters*, 48, e2020GL089991. Available from: https://doi.org/10.1029/2020GL089991

Yukimoto, S., Kawai, H., Koshiro, T., Oshima, N., Yoshida, K., Urakawa, S. et al. (2019) The meteorological research Institute Earth System Model version 2.0, MRI-ESM2.0: description and basic evaluation of the physical component. *Journal of the Meteorological Society of Japan. Ser. II*, 97, 931–965. Available from: https://doi.org/10.2151/jmsj.2019-051

Ziehn, T., Chamberlain, M.A., Law, R.M., Lenton, A., Bodman, R.W., Dix, M. et al. (2020) The Australian earth system model: ACCESS-ESM1.5. *Journal of Southern Hemisphere Earth Systems Science*, 70(1), 193–214. Available from: https://doi.org/10.1071/ES19035

SUPPORTING INFORMATION

Additional supporting information can be found online in the Supporting Information section at the end of this article.

How to cite this article: Ossó, A., Craig, P., & Allan, R. P. (2023). An assessment of CMIP6 climate signals and biases in temperature, precipitation and soil moisture over Europe. *International Journal of Climatology*, 1–22. https://doi.org/10.1002/joc.8169